



3D crustal-scale structure of the West Iberia margin: a novel approach to integrated structural characterization of passive margins

Cristina Granado¹ · Alfonso Muñoz-Martín^{1,2} · Antonio J. Olaiz³ · Oscar Fernández⁴ · María Druet^{1,5}

Received: 3 December 2020 / Accepted: 13 March 2021 / Published online: 28 March 2021
© The Author(s), under exclusive licence to Springer Nature B.V. 2021

Abstract

Hyperextended margins are very heterogeneous along the entire length of the margin, so the definition of tectonic domains made exclusively from 2D seismic sections presents serious limitations. In this work we present an approach of the 3D crustal-scale structure of the West Iberia margin (WIM) by modelling eight lithospheric sections, using seismic, wells and gravity data. The continuous nature of gravity data allowed us to propose a new map of tectonic domains within the WIM. Maps of total horizontal (THD) and vertical gradients (dZ) of Bouguer anomaly have been calculated and compared with other criteria such as the crustal structure and thinning factor. This comparative analysis has been carried out on a section proposed as a model for the Western Iberian Margin (Tugend et al. in *Tectonics*, 2014; Cadenas et al. in *Tectonics* 37:758–785, 2018), and on four 2 + 1/2D gravimetric models transversal to the margin. The results point out a significant variation in the absolute values of Bouguer anomaly, thinning factor and crustal structure along the margin and, therefore, of the position of the different domain boundaries. Clear patterns that correlating the Bouguer anomaly signal and its derivatives to the tectonic domain are evidenced. Most significantly, the necking-zone and its transition to the hyperextended domain are characterized by high values of the THD of the Bouguer anomaly. The observed patterns in Bouguer anomaly and its derivatives provide a solid constraint for mapping the boundaries between different tectonic domains along the margin, even in those areas where limited deep seismic information could lead to uncertain interpretations. The results of this work can also inform on the general kinematics of the WIM.

Keywords West Iberian margin · Hyperextended margin · Tectonic domains · Integrated structural characterization · Gravity modelling

Introduction and objectives

The structure of the West Iberian margin (WIM) (Fig. 1) is heterogeneous along its entire length. This heterogeneity stems from the nature of the pre-rift basement (Murillas et al. 1990), and the added complexity, related to the fact

that its formation involves several rifting episodes and an ulterior partial tectonic inversion (Boillot and Malod 1988).

Classical first-order architecture of this (and other) hyperextended magma-poor rifted margin shows “idealized” cross sections with a set of key rift domains from continent to ocean. Following the terminology proposed by Tugend et al. (2015), five domains were defined based on varying crustal structure, stratigraphic architecture, type of basement, and overall structural style (Fig. 2).

The boundaries between the different tectonic domains of the WIM have been discussed by diverse authors (e.g., Péron-Pinvidic et al. 2013; Welford et al. 2010; Nirrengarten et al. 2018; Druet et al. 2018), based on geophysical and structural criteria, among others the stretching factor, a measure of tectonic stretching and crustal thinning. These criteria are mainly supported by the interpretation of regional reflection seismic sections, by the few well data available, and, to a lesser extent, by potential field data.

✉ Cristina Granado
cgranad@ucm.es

¹ Tectonophysics Group, Earth Sciences Faculty, Complutense University, Madrid, Spain

² Instituto de Geociencias (CSIC, UCM), Madrid, Spain

³ Repsol E&P, Madrid, Spain

⁴ Department of Geodynamics and Sedimentology, University of Vienna, Vienna, Austria

⁵ Instituto Geológico y Minero de España, Madrid, Spain

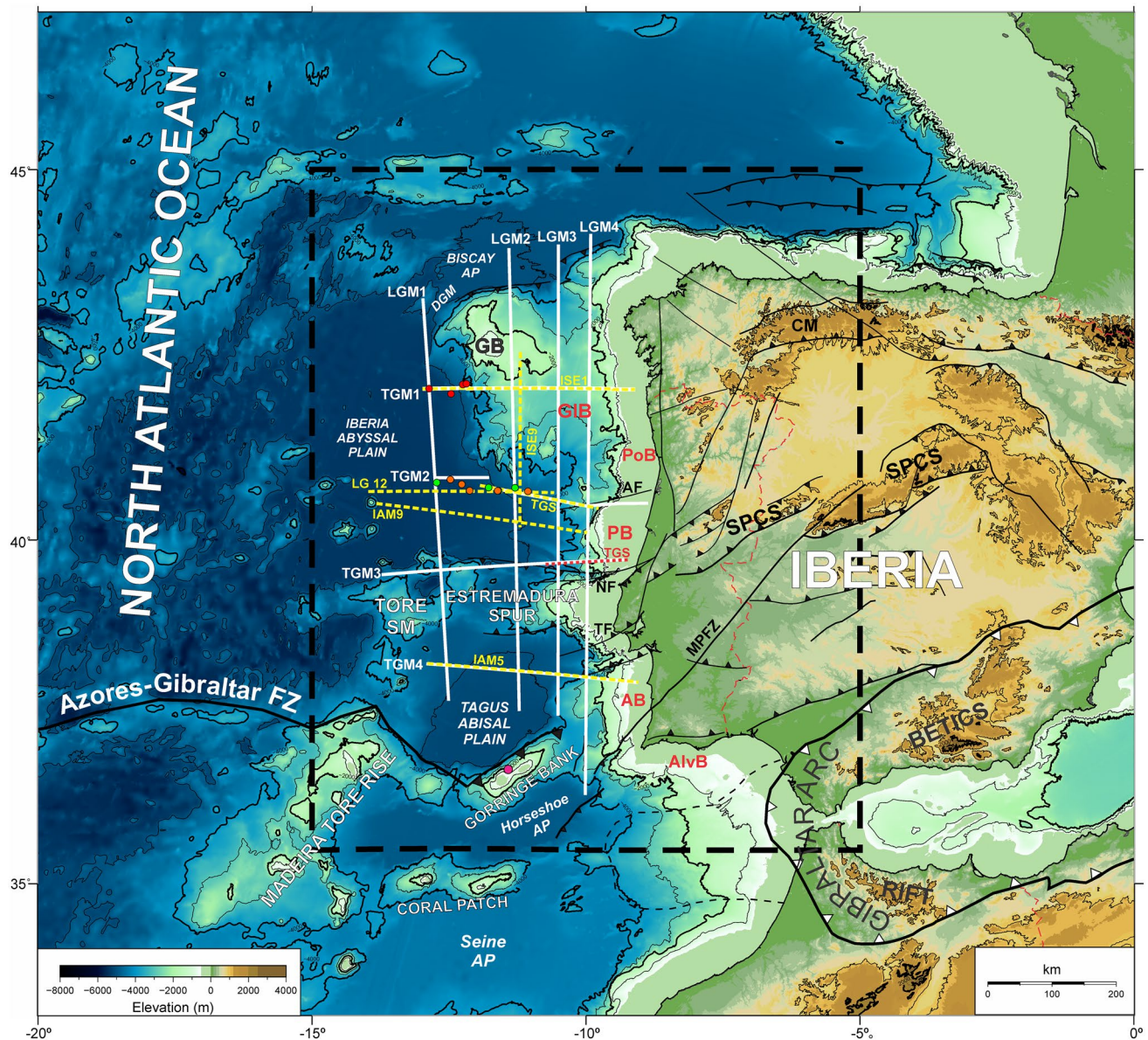


Fig. 1 Tectonic setting of Western Iberian Margin with sedimentary basins and major structures referred in the text. *AF* Aveiro Fault; *NF* Nazare Fault; *TF* Tagus Fault; *AP* Abyssal Plain; *DGM* Deep Galicia Basin; *GB* Galicia Bank; *GIB* Galicia Interior Basin; *PoB* Porto Basin; *PB* Peniche Basin; *AB* Alentejo Basin; *AlvB* Algarve Basin; *MPFZ* Messejana– Plasencia Fault Zone; *SM* Seamount; *FZ* Transform Fault; *CM* Cantabrian Mountains; *SPCS* Spanish- Portuguese Central System. Location of the analyzed transversal and longitudinal lithospheric cross-sections (white thick lines) along the Western

Iberian Margin. Small filled circles show ODP drill holes locations (red, LEG 103; orange, LEG 149; green, LEG 173; pink, site 120). Yellow dashed lines show the locations of seismic profiles used for this work ISE1 (Iberia Seismic Experiment; Zelt et al. 2003); Lusigal 12 (LG12) (with the TGS extension) (Sutra and Manatschal 2012); IAM9 line (Dean et al. 2000); IAM5 (Afilhado et al. 2008) and ISE9 (Clark et al. 2007). Red dashed lines show TGS-Nopec (2 lines integrated with a 2D Austin line) (Sanchez de la Muela et al. 2015)

However, the criteria used to define the different domains does not always coincide among different authors (e.g., Péron-Pinvidic et al. 2013; Mohn et al. 2015; Tugend et al. 2015; Stanton et al. 2016). There are several reasons for this variability: the complexity of the extensional structure, the effects of structural and rheological inheritance on multiple phases of extension, and later geological processes that have

modifying the extensional structure (e.g. compressive reactivation), and the fact that most previous studies have been based on limited/localized 2D seismic data.

This two-dimensional approach hinders lateral correlation between the different structural domains at the regional scale of the margin (Péron-Pinvidic et al. 2015) due to two main factors. Firstly because, regional seismic

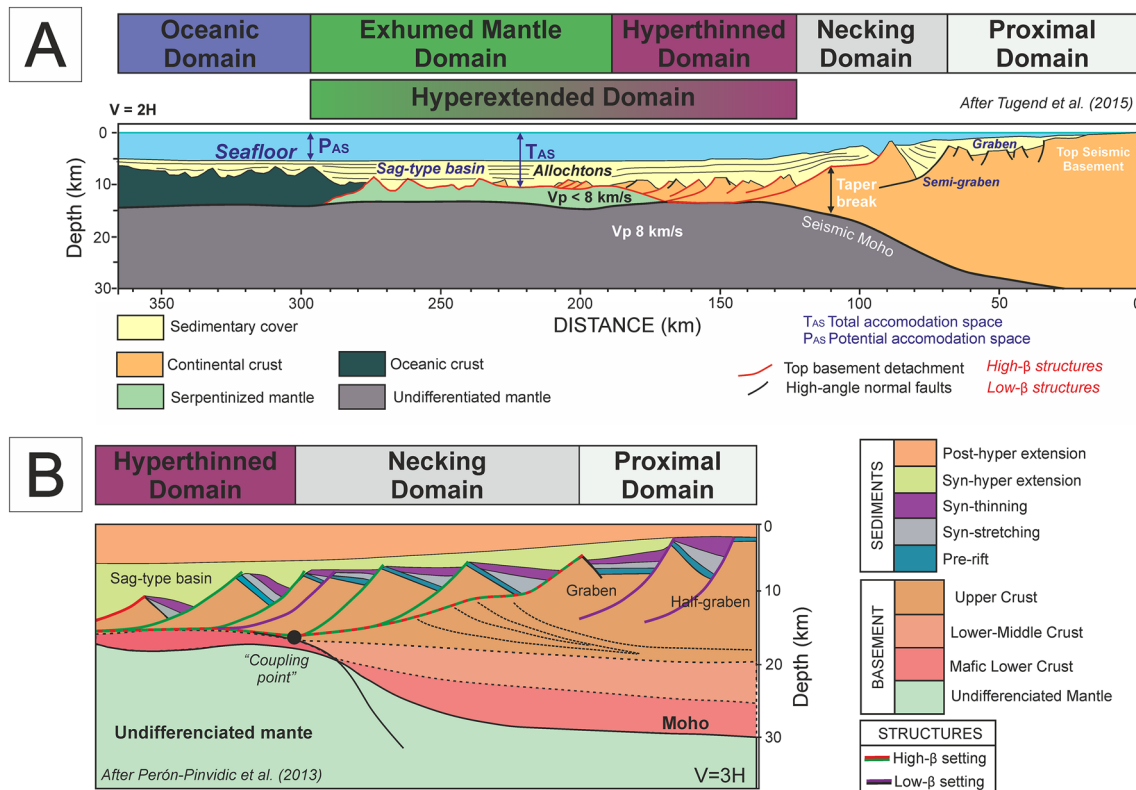


Fig. 2 a Structure of a magma-poor hyper-extended margin. The section includes main elements of each tectonic domain following terminology proposed by Tugend et al. (2015). b Crustal structure, typical

stratigraphic sequence, basement types and main structures that characterize the proximal, necking and hyper-extended domains (modified from Pérón-Pinvidic et al. 2013 and Cadenas et al. 2018)

information is two-dimensional and discontinuous. Secondly because, oblique structures can significantly offset domains from one section to another. The inherent complexity of the extensional system, along with the added complexity caused by tectonic inheritance and posterior tectonic events, adds an extra component of difficulty in generating reliable maps of structural domains from two-dimensional seismic sections only.

In this paper we present an approach with which we have mapped the three-dimensional structure of the WIM at a crustal scale. Crustal scale gravity 2 + 1/2D modelling along key seismic sections, and advanced enhancement tools applied to gravity and magnetic data have been used to enhance, identify, and map the key crustal domains and boundaries of the WIM. Quantifiable parameters (stretching factor, Bouguer anomaly, and gradient values) are subsequently used to propose criteria that can be applied to define the crustal-scale domains the WIM and their boundaries.

The result is a novel map of the WIM in which the structural interpretation of the passive margin is supported by reflection seismic, well drill and gravity data.

Tectonic setting

The WIM (Fig. 1) is located in the southern North Atlantic, just north of the present-day Africa-Eurasia plate boundary (the Azores-Gibraltar Fracture Zone, AGFZ), and its eastward prolongation into the Mediterranean (Srivastava et al. 1990; Zitellini et al. 2009).

The WIM recorded a multiphase rifting history. In a review of the crustal architecture in West Iberia, Pereira et al. (2017), described a complete lithospheric breakup achieved after three to four main rift phases (Rasmussen et al. 1998; Alves et al. 2006, 2009; Pereira and Alves 2011; Mohn et al. 2015). The main rift phases include: (1) Late Triassic-Early Jurassic onset of rifting and widespread segmentation of continental crust; (2) Early Jurassic extension; (3) Late Jurassic to earliest Cretaceous phase of widespread subsidence; (4) Early Cretaceous phase prior to complete continental breakup between Iberia and Newfoundland. As a result, a suite of four syn-rift mega-sequences can be correlated with the conjugate Newfoundland and neighbouring northern Moroccan

margins (Hubbard et al. 1985; Hafid et al. 2000; Pereira and Alves 2012; Ramos et al. 2017). The onset of seafloor spreading occurred in two main pulses: (1) at the end of the Jurassic in the southern segment between the Southern Grand Banks and the Tagus Abyssal Plain (Mauffret et al. 1989; Pereira and Alves 2011) (2) during the Early Cretaceous in the northern segment, between the Iberia Abyssal Plain and northern Grand Banks segment (Tucholke et al. 2007).

After complete continental breakup, West Iberia underwent a period of relative tectonic quiescence in the Late Cretaceous, during which widespread drift sequences accumulated offshore in response to tectonic uplift of the proximal margin (Alves et al. 2009; Pereira and Alves 2012).

During the Cenozoic, the Iberian Peninsula experienced an intense intraplate deformation due to the continuous northwestward movement of the African plate. Initial N-S compression along the northern margin of Iberia from Campanian times (Late Cretaceous) led to the progressive development of the E-W-trending Cantabrian-Pyrenean orogen. Shortening along northern Iberia reached a maximum deformation during the middle Eocene to Late Oligocene (Vergés 1999) and during the Late Oligocene to Early Miocene within the Iberian interior (Curtis 1999; De Vicente et al. 2018).

Ongoing convergence between Africa and Iberia and migration of deformation to the southern Iberian margin led to a climax of intraplate compression within Iberia at ca. 9 Ma (middle Tortonian, Dewey et al. 1989). This caused renewed uplift of the Central System (Fig. 1) in the onshore and offshore (Cunha 1992; De Bruijne and Andriessen 2002; Ribeiro et al. 1990) and of the mountains of NW Portugal, mainly by reverse faulting and thrusting (Cunha 1992; Cunha et al. 2000).

West Iberian Margin (WIM)

The WIM is the rifted margin flanking western Iberia. In the north (GB, DGM, Fig. 1), the WIM is characterized by a broad domain of extended continental crust that stretches around 300 km from the coast out to a domain of exhumed subcontinental mantle beyond the Galicia Bank region (Boillot et al. 1987; Druet et al. 2018). Further south (IAP, Fig. 1), the continental crust only extends some 200 km from the coast or less before transitioning into the domain of exhumed mantle (Pereira et al. 2017).

The WIM has a roughly N-S trend and is segmented by a series of regional-scale structures, which act as boundaries to the main basins on the margin. Two first-order tectonic lineaments, the Messejana-Plasencia Fault Zone and the Nazare Fault Zone, divide the continental Western Iberian shelf into two distinct segments, namely SW Iberian margin (Alentejo Basin) and the NW Iberian margin (including the

Lusitanian, Peniche, Porto and Galicia Basins) (Fig. 1). The Messejana-Plasencia Fault Zone, located in SW Iberia, is a 500-km-long NE-trending transcurrent fault zone formed during the Late Palaeozoic that was later reactivated during Mesozoic rifting and Cenozoic inversion (e.g. Schermerhorn et al. 1978; De Vicente et al. 2018). This fault zone separates the WIM from the southwest Iberian margin (Algarve Basin). The Nazare Fault Zone extends over 250 km from onshore to the continental slope. It separates the SW from the NW Iberian margin, and controls deposition and structural trends in the Lusitanian Basin and northern Estremadura Spur (Wilson et al. 1989; Alves et al. 2009). Additionally, two strike-slip zones might have played a significant role in margin segmentation (namely the Aveiro and the Tagus Faults, Pereira et al. 2017).

The distal WIM in turn can be subdivided into three physiographic provinces (Fig. 1). A northern segment is characterized by the Galicia interior basin (GIB), the Galicia Bank region (GB), and the Deep Galicia Margin (DGM). The GIB is a N-S trending structural low, located westward of the Galician continental shelf, with an approximate width of 100 km. It developed in response to Early Cretaceous NNW-SSE normal faulting (Murillas et al. 1990). West of the GIB, the GB region is a structural high underlain by poorly extended continental crust (Whitmarsh and Sawyer 1996). Westwards the Deep Galicia Margin (DGM) includes the distal part of the margin and the continent-ocean transition (Manatchal and Bernoulli 1999) characterized by extremely extended continental crust blocks with a thin sedimentary cover, underlain by an ultramafic basement. This region ends westwards in a serpentinized peridotite ridge (Boillot et al. 1987). The ultramafic basement of the DGM originated by subcontinental mantle exposure during the final stages of rifting (Krawczyk et al. 1996; Kornprobst and Chazot 2016).

The central segment of the distal WIM is formed by the Iberia Abyssal Plain (IAP). This plain lies southwest of the GB and is bounded to the south by the Estremadura Spur that separates it from the Tagus Abyssal Plain (Pinheiro et al. 1996; Fig. 1). To the west and northwest, the limits of the IAP are roughly defined by the 4800-m isobath, which approximately marks the transition from the flat topography characteristic of the IAP to the irregular morphology typical of oceanic basement further west.

Finally, the southern segment of the distal WIM is occupied by the Tagus Abyssal Plain (TAP). This plain is surrounded by three major ridges: the Madeira-Tore Rise in the west, the Estremadura Spur in the north, and the Gorringer Bank in the south. The Tagus Abyssal Plain represents the Jurassic oceanic portion of the WIM, with a transition to continental crust which is inferred to occur in the eastern half of the deep-sea plain (Pinheiro et al. 1992). An alternative view, implying that the basin is floored by exhumed mantle rocks, as opposed to oceanic crust, has been recently

proposed (Bronner et al. 2011). However, this point is still debated (Tucholke and Sibuet 2012). In the Tagus Abyssal plain, the J anomaly occurs over a basement showing a seismic velocity structure characteristic of oceanic crust (Afilhado et al. 2008) that is thickened at the magmatic Madeira-Tore Rise (Nirrengarten et al. 2017).

The J anomaly is well defined south of AGFZ within an oceanic spreading system, associated with Mesozoic isochrons (Tucholke and Ludwig 1982), but its origin north of the AGFZ is still debated and the amplitude decreases northwards and fades out west of Galicia Bank (Nirrengarten et al. 2017).

The J anomaly north of the AGFZ, has been considered in the past as an oceanic anomaly corresponding to the M4, M3 or M0 isochron (Whitmarsh and Miles 1995; Sibuet et al. 2004) or a transition from an exhumed mantle domain to a more magmatic oceanic crust (Bronner et al. 2011). Nirrengarten et al. (2017) recently rejected this idea and conclude that the J-anomaly is the result of polygenic and multiple magmatic events occurring during and after the formation of the first oceanic crust. Sanchez et al. (2019) pointed that the origin of volcanic edifices along the Tore-Madeira Ridge could be considered oceanic and exhumed mantle, and their orientations are not aligned with the previously interpreted oceanic magnetic anomaly M0.

M3 (124My) can be modelled by seafloor spreading, at rates of $\sim 10\text{--}14$ mm year⁻¹. (Whitmarsh and Miles 1995; Whitmarsh et al. 1996; Dean et al. 2000; Russel and Whitmarsh 2003). Previous modelling of magnetic anomalies and seismic velocities indicated that this region has seafloor spreading magnetic anomalies and the seismic velocity structure characteristic of oceanic crust, albeit perhaps slightly thinner than normal; magnetic modelling suggested that it was formed from the time of anomaly M3. This interpretation is supported by the discovery at ODP site 1070 of a 119 Ma pegmatite gabbro and gabbro veins, which were cored in the basement without encountering basaltic rocks (ODP Leg 173 Shipboard Scientific Party 1998; Manatschal et al. 2001; Whitmarsh & Wallace 2001).

Rift domain terminology

Regardless of their variability, Atlantic magma-poor rifted margins share many first order similarities (e.g., Reston 2009; Péron-Pinvidic et al. 2013). In some studies, these rifted margins are characterized from continent to ocean by five structural domains, which are referred to as proximal, necking, hyperthinned, exhumed mantle, and oceanic domains (Fig. 2) (Tugend et al. 2015). The hyperthinned and exhumed mantle domains are referred together as the distal domain (Péron-Pinvidic et al. 2013) or hyperextended domain (Tugend et al. 2015).

These five rift domains are characterized by different structures, particular basin geometries and basement type (Fig. 2), suggesting that they result from different modes of deformation (Sutra et al. 2013) that migrate progressively toward the area of the future breakup (Péron-Pinvidic and Manatschal 2009). The boundaries between domains are commonly considered as transitional rather than sharp, which may hamper their identification in some settings. This is related to the fact that the domains are associated with specific deformation processes that can overlap (and interact) in time and space (Péron-Pinvidic et al. 2013). In reactivated magma-poor rifted margins, the mapping of rift domains can provide important constraints about the rift architecture (Tugend et al. 2014), thus facilitating quantitative restoration of hyperextended domains (Sutra et al. 2013) in the absence of well-constrained magnetic anomalies (Nirrengarten et al. 2017).

The *proximal domain* is characterized by classical graben and half-graben basins as a result of minor lithospheric thinning (Sutra et al. 2013; Tugend et al. 2015). Basement top and the Moho are approximately parallel (Péron-Pinvidic and Manatschal 2009). Deformation is decoupled, with brittle faults in the upper part of the crust detaching at mid-crustal depth (decoupling level), and with the lower continental crust exhibiting ductile behaviour (Sutra et al. 2013). Due to moderate thinning, little accommodation space is created (Sutra et al. 2013). The continental crust is interpreted to be > 25 km thick at the transition into the necking domain (Dean et al. 2000).

The *necking domain* has been defined as the area where 30 (± 5) km continental crust is thinned to about 10 km (Mohn et al. 2012; Péron-Pinvidic and Manatschal 2009; Sutra et al. 2013) (Fig. 2b). Crustal thinning results in the shallowing of the Moho, the deepening of the top basement and the creation of significant amounts of accommodation space, recorded by progressive thickening of the syn-rift sequences and deepening of depositional environments (Tugend et al. 2015). The outboard limit of this domain corresponds to a break in the crustal taper geometry, where crustal thickness is reduced to the order of 10 km or less (Osmundsen and Redfield 2011) (Fig. 2a). This usually coincides with the coupling point (Pérez-Gussinyé and Reston 2001; Sutra et al. 2013; Péron-Pinvidic et al. 2013; Nirrengarten et al. 2017). The coupling point represents the location where crustal deformation changes to involve the entire upper and lower crusts (coupled deformation), with faults penetrating across the thinned crust directly into the mantle (Sutra et al. 2013), due to the embrittlement of the lower crust (Pérez-Gussinyé and Reston 2001).

Within the *hyperextended domain*, crustal thickness is less than 10 km. Extreme crustal thinning leads to the generation of a substantial amount of accommodation space (Tugend et al. 2015). Extensional faults penetrate and

exhume the continental lithospheric mantle under a simple shear regime (Pérez-Gussinyé et al. 2003; Sutra et al. 2013; Doré and Lundin 2015), and serpentinization of the lithospheric mantle may occur (Pérez-Gussinyé and Reston 2001). As tectonic thinning progresses, the serpentinized mantle may be exposed and may crop out on the seafloor and overlain directly by sediments (e.g.; Boillot et al. 1987 and 1988; Sutra et al. 2013). Local magmatic additions, continental-derived extensional allochthons, serpentinized mantle rocks, locally reworked in syntectonic breccias, and sag-type basins filled by thick aggradational and progradational sequences that wedge out oceanward, are also typical features of this domain (Tugend et al. 2015) (Fig. 2a).

In this work we differentiate the *hyper-thinned domain* (where a thinned continuous continental crust remains) from the *exhumed mantle domain* (where a serpentinized mantle with only isolated continental cortical blocks appears below the sediments).

The establishment of stable oceanic spreading and the presence of seafloor-spreading magnetic anomalies characterize the *oceanic domain* (Eagles et al. 2015; Cadenas et al. 2018). The landward limit of this domain remains strongly debated owing to the gradational character attributed to breakup (Péron-Pinvidic and Manatschal 2009) and the uncertainties in the interpretation of magnetic anomalies within ultra-distal rifted margins (Sibuet et al. 2007; Nirrengarten et al. 2018; Fernández et al. 2020).

Data sources and methodology

In order to carry out a regional study including all the Western Iberian Margin with different types of data, it has been necessary to use and homogenize various sources of information and databases. In this way the information is comparable throughout the range with enough resolution. Used data in this work come from diverse sources.

Bathymetry/topography

Bathymetry, used in Figs. 1 and 11a, is from the 2018 version of the EMODnet digital terrain model (DTM) (<http://portal.emodnet-bathymetry.eu/>). EMODnet DTM released with a grid resolution of 1/16 * 1/16 arc-minutes using the best available bathymetry data sets from an increasing number of data providers. This DTM included data from plummets, single beam, multi beam, and LIDAR observations, from composite DTMs and Satellite Derived Bathymetry for selected coastal stretches. To prevent gaps in the EMODnet DTM layer, these areas have been filled with the GEMCO 2014 data.

Seismic data

Available multichannel seismic (MCS) reflection profiles, seismic refraction profiles, as well as deep seismic soundings (DSS) within the study area were compiled in order to construct representative regional transects for crustal-scale gravity modelling.

ISE1 (Iberia Seismic Experiment; Zelt et al. 2003) was acquired in 1997 and first published and discussed by Zelt et al. (2003) and Henning et al. (2004).

Lusigal 12 (LG12) line across the Southern Iberia Abyssal Plain was acquired in 1990 (Boillot 1990; Beslier 1996) with the TGS extension (Sutra and Manatschal 2012).

IAM9 line is a long wide-angle seismic profile acquired in the southern Iberia Abyssal Plain (Dean et al. 2000).

IAM5 is a 370 km long seismic transect acquired and interpreted by Afilhado et al. (2008) that includes a multi-channel near-vertical and wide-angle reflection data.

ISE9 is a 200 km long N-S multichannel seismic reflection and ocean bottom seismometer reflection/refraction section (Clark et al. 2007).

TGS-Nopec data (2 lines integrated with a 2D Austin line) that was first published in Sutra et al. (2013) and after modeled by De la Muela et al. (2015).

Moho geometry

Regional-Scale Moho geometry has been obtained from several sources: GOCE Exploitation for Moho Modeling and Applications (GEMMA) Project (Reguzzoni and Sampietro 2015) and Diaz et al. (2016). Moho topography beneath the Iberian-Western Mediterranean region mapped from controlled-source and natural seismicity surveys. We constrain the regional Moho-models with the Moho geometry along the deep seismic sections cited above.

Sediment thickness

For the sediment thickness where no well data or seismic profiles are available, we used a database for the world's oceans compiled by the NOAA at the National Geophysical Data Centre (Whittaker et al. 2013), which consists in a grid with spacing of 5 arc minutes and represents the most recent regional database available.

Well data

Well data comes from hydrocarbon exploration wells, Deep Sea drilling Project wells (DSDP) Leg 13, Site 120, and Ocean Drilling Program wells (ODP) Legs 149 (Sawyer et al. 1994), 173 (Whitmarsh et al. 1998) and 103 (Boillot

et al. 1987), as well as dredge data (Baldy 1977; Matos 1979; Mougénot et al. 1979). We describe the particular constraints used in each gravity model below (Sect. 4).

Gravity data

As the gravity anomalies are largely affected by the bathymetry and topography, we calculated the Bouguer anomaly. Gravity Onshore Bouguer gravity anomalies (BA) have been taken from a recent compilation of gravity data on Iberia, *Topo-Iberia project* (Ayala 2013). Offshore Bouguer gravity anomalies come from Spanish Economic Exclusive Zone Project obtained between 2001 and 2008 (Druet et al. 2019) and Multi-Satellite Altimeter Gravity Program (Multi-Sat) GETECH 2016 compilation data. The Bouguer anomaly was obtained by subtracting the gravity contrast produced by the water–sediment from the Free-air anomaly grid, using densities of 1.03 g/cm^3 for the water layer and 2.67 g/cm^3 as a mean value for the Bouguer Slab.

Gravity reduction has been executed with the WGS84 Ellipsoidal Gravity Formula, and the final Bouguer anomaly

includes sea-bottom and terrain correction (Carbó et al. 2003; Kane 1962; Nagy 1966). The used density for the upper terrain level was 2.2 g/cm^3 and it was selected after checking different density values along several profiles across bathymetric features. This sea-bottom and terrain correction was carried out up to 20 km using 200 m-size Digital Elevation Model for proximal correction (until 5 km) and 1 km size for distal correction. The final complete Bouguer anomaly grid was calculated with the continuous curvature splines in tension method (Smith and Wessel 1990) using GMT software (Wessel and Luis 2017), with a tension parameter of 0.25 and 2-min interval regular grid (Fig. 3).

Magnetic data

The magnetic anomaly datasets used in this study are from World Digital Magnetic Anomaly Map version 2.0 (Lesur et al. 2016). We applied the reduction to the magnetic pole for a better comparison with gravity data, using the same parameters as in Miles et al. (1996) for Iberia. The final regular grid was calculated with the continuous curvature

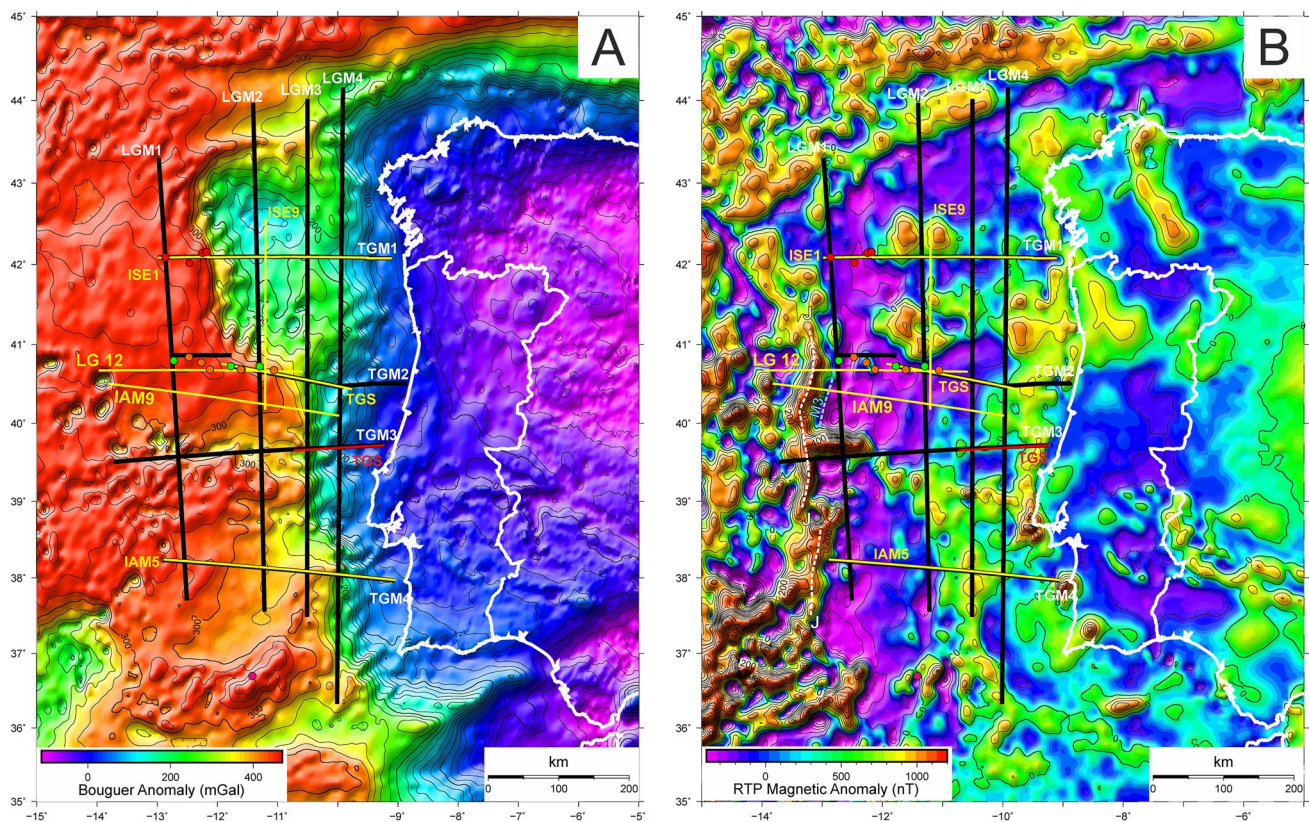


Fig. 3 **a** Complete Bouguer anomaly map, and **b** Reduced to the Pole (RTP) Magnetic anomaly map of the WIM. Magnetic data have not been used in the modelling, but we have used these data to locate and constrain the oceanic crust beginning as well as the igneous intrusive bodies. Location of modelled lithospheric cross-sections, ODP

drill holes locations and main seismic lines are shown. On the RTP magnetic anomaly map J-magnetic anomaly (white dash line) and M3 isochrone (blue dash line) have been plotted. (See text for data descriptions and sources)

splines in tension method (Smith and Wessel 1990) using GMT software (Wessel and Luis 2017), with a tension parameter of 0.25 and 2-min interval regular grid (Fig. 3).

Use of gravity tools to define boundaries between tectonic domains

The use of gradients and filters is a common tool to enhance data, as well to assist interpretation of geophysical data. Gradient or derivative filters resolve variations in the geophysical response with distance, with time, or with frequency. They are valuable in locating subtle changes in the gravity field.

Horizontal gradients are very sensitive to the edges of bodies and are ‘edge detectors’. These gradients emphasize changes in the measured parameter, but only in the direction in which they are calculated, so changes in geology oriented perpendicular to the gradient direction produce the strongest gradient response. They -x and -y oriented gradients can be combined as the square root of the sum of the squares of the derivatives to form the Total Horizontal Derivative (THD) (Blakely 1996). The THD (Fig. 4a) represents the maximum gradient in the vicinity of the observation point and, therefore, is perpendicular to contours of the measured parameter, and peaks over lateral contacts, or forms a ridge if the

source is narrow. This enhancement creates a band along the lateral limits of the body, delineating the lateral density contrast (Dentith and Mudge 2014). The vertical gradient (dZ) (Fig. 4b) is simply the result of calculating the first derivative of the anomaly in the vertical direction and enhances the position of the minimum or maximum anomaly zones generated by the bodies with property contrast (Blakely 1996).

Upward continuation is a smooth, low-wavenumber pass filter which emphasizes the anomalies from the broader, deeper sources at the expense of the shallow-sourced anomalies and noise in the anomaly field (Hinze et al. 2013). 20 km of height for the upward continuation to achieve an appropriate image of the crust was proposed in Angola and Gabon margins (Fernández et al. 2020). Therefore, enhancement observed anomalies are mainly depicting the Crust-Mantle boundary. We have applied an upward continuation of Bouguer anomaly grid before to calculate both the THD and dZ due to the regional scale of this work.

Forward modelling and geophysical/geological constraints

Available multichannel seismic reflection profiles and Deep seismic soundings (Fig. 1) within the study area were compiled in order to construct representative regional transects

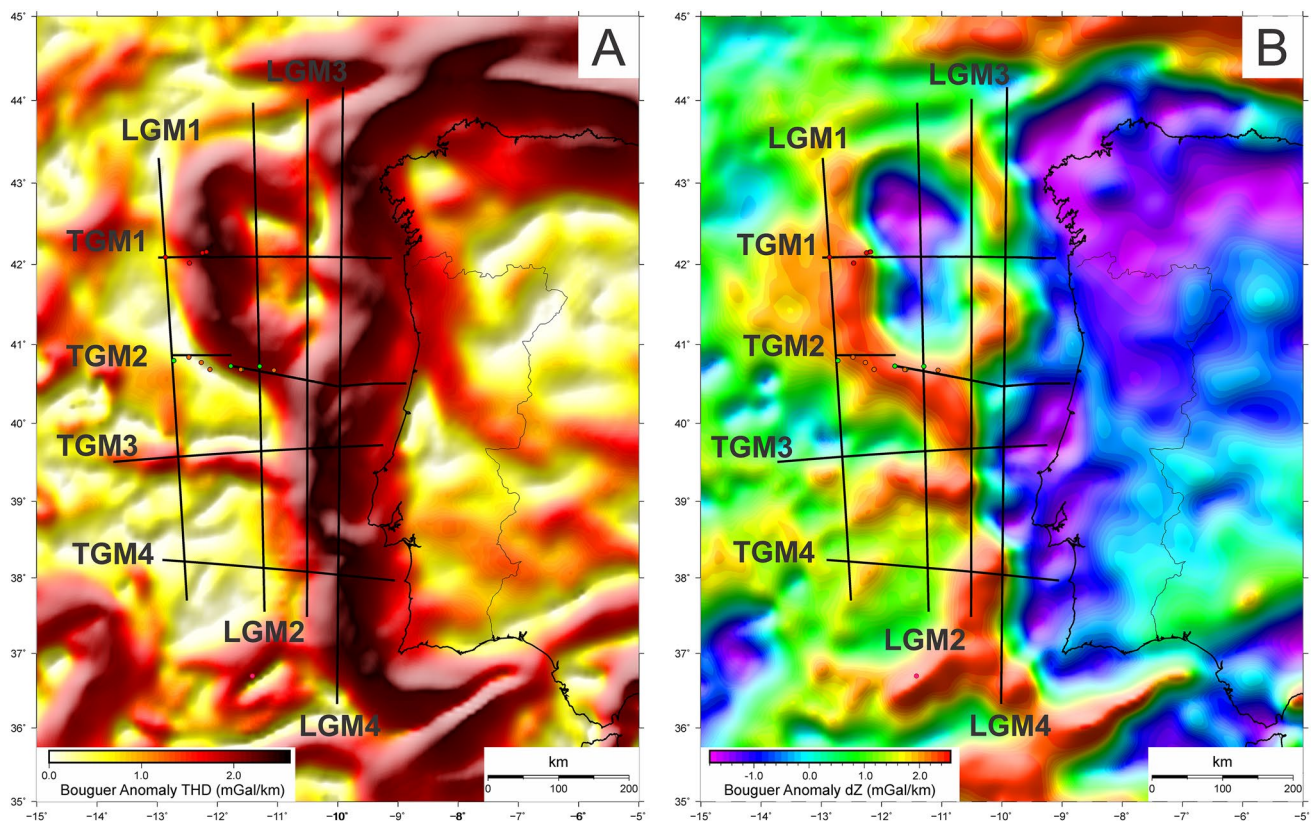


Fig. 4 Total Horizontal Derivative (a) and vertical derivative (b) of Bouguer anomaly along WIM

for crustal-scale gravity modelling. Finally, four transversal (E-W) and four longitudinal (N-S) 2 + 1/2D density models were performed along the Western Iberia Margin, in order to analyze the 3D structure (Figs. 1 and 3). The location of gravity models is conditioned by the existing seismic profiles and IODP sites to constrain them and they are drawn normal to the main gravity anomaly changes.

We used the GMSYS commercial package integrated with Geosoft Oasis Montaj to perform the 2D forward modelling. Calculations of the gravity model response are based on the standard iterative methods and algorithms (Talwani and Heirtzler 1964; Talwani et al. 1959; Won and Bevis 1987). The transverse extension of the modeled blocks has been made considering the lateral extension of Bouguer anomalies, and THD and dZ maps, and it oscillates between 20 km and more than 100 km.

Most of the gravity models constructed during this study are supported by multichannel reflection seismic profiles (MCS) and also by previous deep reflection and refraction seismic profiles carried out by previous authors and cited above. Refraction seismic profiles have been used to constrain the crustal density structure and differentiate upper and lower crust (based on seismic velocities) and to define the depth to the Moho. To set Moho depth where no refraction seismic information is available, we have used the Moho depth model published by Diaz et al. (2016), and that derived from the GOCE satellite data (GEMMA Project; Reguzzoni and Sampietro 2015) as starting point for modelling. It must be noted that the GEMMA model is a low-resolution global model that shows correlation errors in continental margins. These misfits are due to a simplistic description of the oceanic seafloor used for the model and, locally, to a lack of seismic observations (Sampietro et al. 2013). This procedure has allowed modelling first-order structures that imply an important lateral density contrast, such as those of the continent-ocean transition and Moho geometry. Modelling the first-order tectonic features along the whole WIM allows the comprehension of the margin structure at large regional scale.

Due to the regional scale of this work, 15 different density units are distinguished on it. Sedimentary units established from high resolution seismic data (Table 1) have been rearranged. Their densities have been calculated from wide angle seismic velocities (González et al. 1999; Banda et al. 1995; Sibuet et al. 1995; Krawczyk et al. 1996; Whitmarsh et al. 1996; Dean et al. 2000; Pérez-Gussinyé et al. 2003; Zelt et al. 2003; Henning et al. 2004; Afilhado et al. 2008; Jiménez-Munt et al. 2010 and Sutra et al. 2013) based on Barton 1986; Brocher 2005; Christensen and Mooney 1995; Ludwig et al. 1970). Differentiated units are shown in Table 1 and in Fig. 5.

Gravity models have been adjusted in a stepwise manner. The process has started by fixing the interpretation of the

Table 1 Density values assigned to different seismic velocities following empiric relationship curves (Barton 1986; Brocher 2005; Christensen and Mooney 1995; Ludwig et al. 1970)

Units	Density (g/cm ³)	Seismic velocity (km/s)
Water	2.67	1.5
Post-rift sediments	2.2	2
Syn-rift sediments	2.3	2.5
Jurassic sediments	2.4–2.6	4–4.5
Triassic sediments	2.55	4.5
Triassic salt	2.1	2
Upper continental crust 1	2.6–2.65	5–5.5
Upper continental crust 2	2.7–2.75	6
Upper continental crust 3	2.8–2.85	6.5
Intrusive rock	2.7–2.9	6–6.6
Lower continental crust	2.85–2.9	6.6
Upper oceanic crust	2.8	6.5
Lower oceanic crust	3	7.4
Highly serpentinized mantle	2.6–2.85	5.7–6.5
Medium serpentinized mantle	2.9–3.1	7.5
Mantle	3.3	8

Used seismic velocities from (Córdoba et al. 1987; Banda et al. 1995; Sibuet et al. 1995; Krawczyk et al. 1996; Whitmarsh et al. 1996; Dean et al. 2000; Pérez-Gussinyé et al. 2003; Zelt et al. 2003; Henning et al. 2004; Afilhado et al. 2008; Jiménez-Munt et al. 2010; and Sutra et al. 2013)

shallow part of the structure, based on well and MCS data. Crustal body and Moho geometry have been initially based on deep reflection and refraction seismic sections and on the GEMMA regional model (Reguzzoni and Sampietro 2015). On this initial model, the mismatches between the measured gravity and the gravity curves generated from the density model were analyzed. The adjustment between both curves has begun with the larger wavelength, starting by adjusting the Moho (or top of mantle) geometry. After this, where necessary, the geometry of the top of the basement or the geometry of the upper and middle crust has been modified. Finally, and only in some cases, it has been necessary to modify the densities assigned to some blocks of the upper crust, always taking into account reflection seismic data and previous works.

Misfits are observed in the models. There are several possible sources:

- Density values taken from bibliography are assumed for the units where not direct observation or velocity/density relationships exist.
- 2D potential fields modelling assume that the properties (density, velocity or magnetic susceptibility) are constant for the whole block, in both vertically and laterally. This limitation is overcome by using 3D inversion. However,

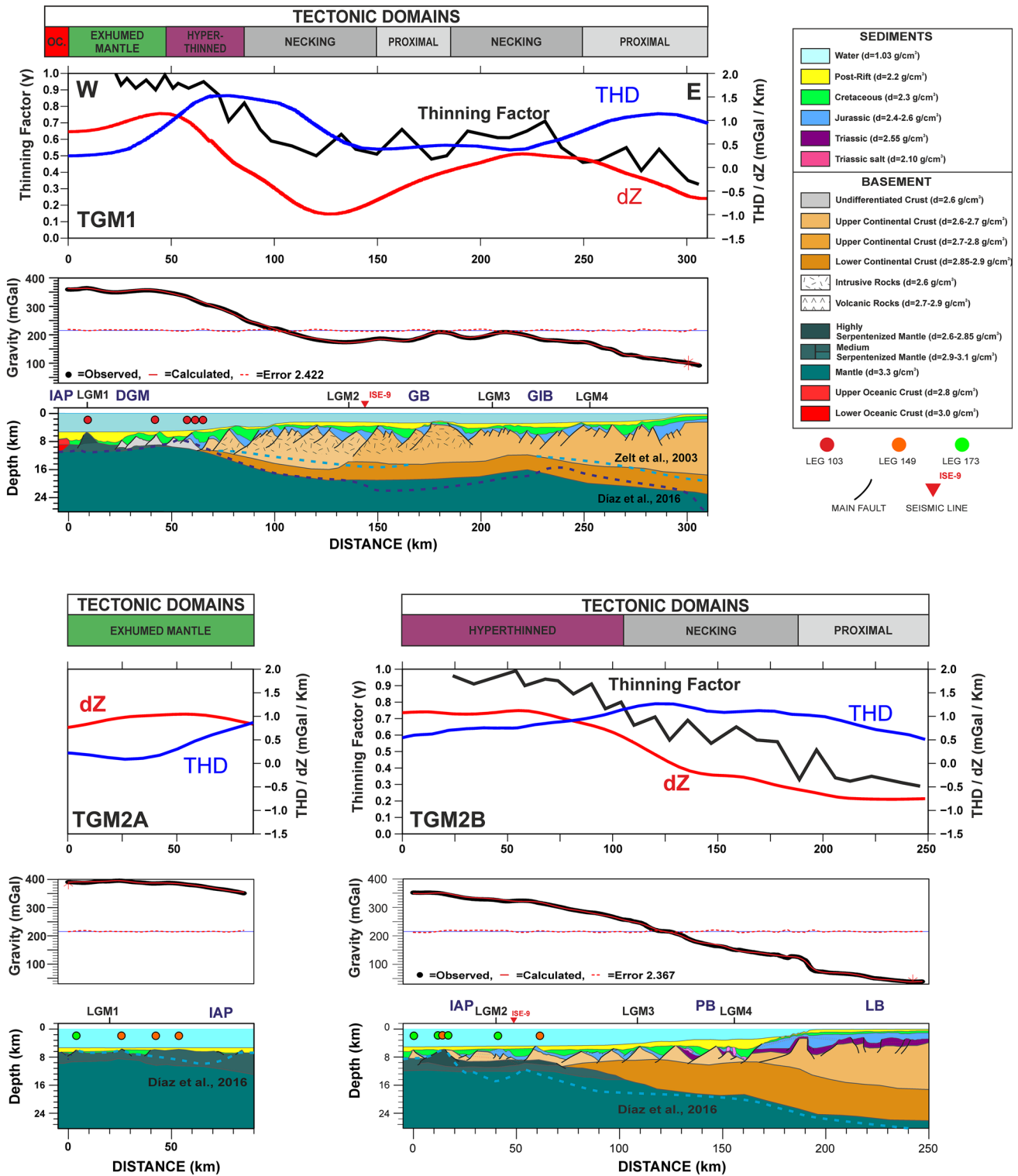


Fig. 5 Adjusted transversal Gravity models TGM1 and TGM2 (see location on Figs. 1 and 3). Some horizons from previous published authors are plotted (and referenced) over the gravity model (dashed coloured lines) The base of the upper crust and the Moho along the northern ISE1 profile were constrained by refraction data of the ISE1 profile (Zelt et al. 2003). Above the models: Thinning Factor

(γ), Total Horizontal (THD) and Vertical (dZ) derivatives of Bouguer anomaly calculated along the sections have been plotted. Top: Proposed Tectonic domains distribution (See text for the explanation). *GIB* Galicia Interior basin; *GB* Galicia bank; *DGM* Deep Galicia Margin; *IAP* Iberia abyssal plain; *LB* Lusitanian basin; *PB* Peniche basin

if a huge amount of microblocks is created to reduce the misfit and their presence is not constrained by external geological and/or geophysical data, the resultant model may have a perfect match but not geological sense.

- Potential field modelling has the property of non-uniqueness solution. That means that different sources can generate the same signal, depending of its density/magnetic susceptibility contrast, depth, size.

The stretching (β) and thinning (γ) factors

McKenzie's (1978) model is a widely used method to relate crustal stretching, subsidence, and heat flow during passive rifting. The key term in the model is the stretching factor ($\beta = L/L_0$) which is defined as the ratio of the final length, L , to the initial length, L_0 , of the lithosphere for any increment of lithospheric stretching. This factor is proportional to the subsidence of a rift basin, which is in turn controlled by faulting in the upper crust. As originally proposed, β is usually determined by solving for the best fit of the modeled tectonic subsidence curve to the back-stripping curve calculated from borehole and/or seismic data (Steckler and Watts 1978). But as crustal thickness profiles from seismic and gravity data have become more widely available, direct estimates for crustal thinning have been used to calculate β (Reston et al. 2007; Reston 2009; Reston and McDermott 2014).

Another way to approach the rifting and subsidence process is via the *thinning factor* (γ), which accounts for how much the thickness of the block decreased during a certain amount of stretching, varying from 0 (no thinning) to 1 (100% of thinning) (Hellinger and Sclater 1983; Davis and Kusznir 2004). By describing a pre-rift block that has an initial length equal to its initial thickness ($L_0 = t_0$), one can calculate the thinning factor that is equivalent to the crustal stretching factor, as given by:

$$\gamma = \frac{t_0 - t_f}{t_0} = 1 - \frac{1}{\beta} \quad (1)$$

In this work we have selected the thinning factor (γ), to compare the degree of crustal stretching along the whole WIM, because it is a factor that goes from 0 to 1 and allows its simplest comparison with values of Bouguer anomaly and gradients. We have used 30 km as initial crustal thickness (t_0) before rifting (Diaz et al. 2016).

Results: structure and tectonic domains along the WIM

Here we present the adjusted gravity models. The different sections are described from north to south for the transverse cross sections and from west to east for the longitudinal ones. All transverse models have the same vertical scale exaggeration ($\times 2$). Longitudinal models have a $4 \times$ vertical exaggeration. All models have been represented with the same range of anomaly and gradients variations in order to be easily compared. Finally, for each model, we compare the *thinning factor*, and both the THD and dZ Bouguer anomaly values with the modeled structure, in order to establish criteria to define the tectonic domains.

Transversal gravity models

All Transversal gravity models (Figs. 5 and 6) show a proximal domain characterized by 20 to 26 km thick continental crust (similar to Zelt et al. 2003; Dean et al. 2000; Afilhado et al. 2008). The boundary between the proximal and necking domains is associated with the presence of major extensional faults that cross-cut into the lower continental crust and contributes to the thinning and exhumation of the lower crust. The necking domain is characterized by a progressive rise of the Moho and a drop in the depth to the top of the basement across normal faults. The hyperthinned domain is defined where faults are interpreted to cut across the entire continental crust into the mantle (coupling of deformation) or where continental crust thins to less than 10 km. Along the hyperthinned domain the continental crust is stretched and delaminated until the lower crust disappears. Westwards a high-density unit of serpentized mantle is modeled, with some undifferentiated small continental crustal blocks resting on it. The densities of the serpentized bodies are variable depends on the degree of serpentization. In this work, we evaluate quantitatively the degree of serpentization using existing seismic velocity models (Zelt et al. 2003; Dean et al. 2000; Sallarès et al. 2013), identifying a highly serpentized mantle unit (from 2.6 to 2.85 g/cm³) and a medium serpentized mantle unit (from 2.9 to 3.1 g/cm³) assuming a total thickness of 5–6 km, that correlated well with the thickness observed through the seismic sections (e.g. IAM9 seismic section at the IAP; Pinto et al. 2016).

Magnetic data suggest the limit with oceanic domain must be at the western end of each section, usually associated with the first well-defined magnetic anomaly. We discuss the criteria used for this limit below (Sect. 5).

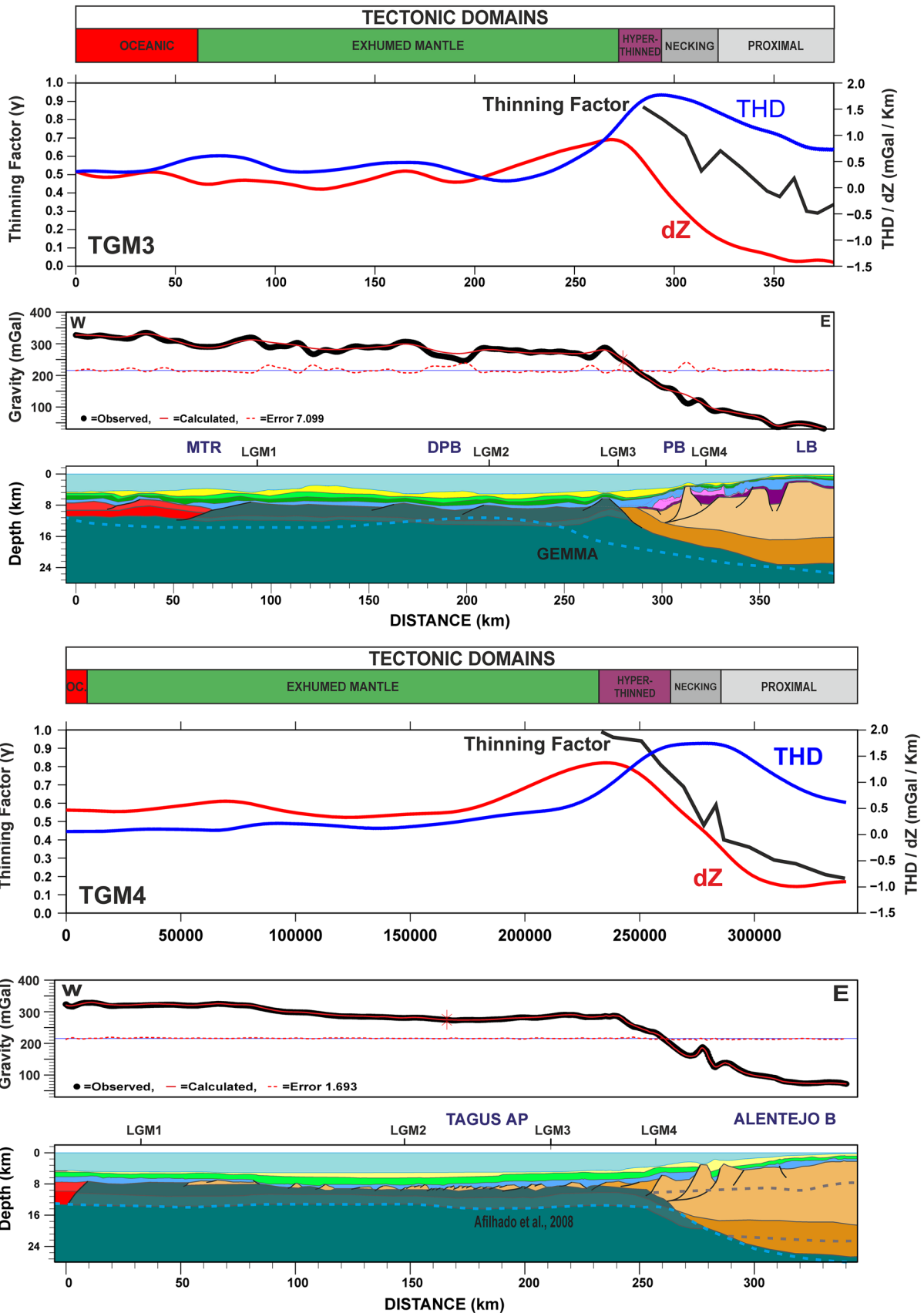


Fig. 6 Adjusted Gravity models TGM3 and TGM4 (see location on Figs. 1 and 3). Some horizons from previous authors are plotted (and referenced) over the gravity model (dashed coloured lines) the deep structure is constrained with seismic velocity models from Afilhado et al. (2008). Above the models: Plot of calculated Thinning Factor (γ), Total Horizontal (THD) and Vertical (dZ) derivatives of Bouguer anomaly along the sections. Top: Proposed Tectonic domains distribution (See text for the explanation). *LB* Lusitanian basin; *PB* Peniche basin; *DPB* Distal Peniche basin; *MTR* Madeira-Tore rise; *Tagus AP* Tagus abyssal plain; *Alentejo B* Alentejo Basin

Transverse Gravity Model 1 (TGM1) (Fig. 5)

Gravity model TGM1 crosses the main Early Cretaceous rift structures of the west Galicia margin, including the Galicia Interior Basin (GIB), Galicia Bank (GB) and ends in the Deep Galicia Margin (DGM, Figs. 1 and 5). It is supported by refraction and reflection seismic and ODP data described above (Boillot et al. 1987; Sibuet et al. 1995; Whitmarsh et al. 1996; González et al. 1999; Pérez-Gussinyé et al. 2003). Mesozoic and Cenozoic sediment sequences are constrained by the re-interpretation of ISE 1 seismic reflection made by previous authors (Manatschal 1999, 2015; Reston 2007; Sutra and Manatschal 2012; Mohn 2015; Amigo-Max et al. 2019). The base of the upper crust and the Moho along the northern ISE1 profile were constrained by refraction data of the ISE1 profile (Zelt et al. 2003).

The WIM is over 250 km wide on this section. Continental crust thins from over 20 km in the proximal domain near the coast, down to just over 10 km thickness in the GIB. Eastward, the continental crust thickens again to over 15 km on the GB, and thins again progressively into the DGM. Based on the crustal thickness of the GB and the geometry of the faults, detaching within the middle crust, it is interpreted that the GB corresponds to a proximal domain. The thinned crust in the GIB is interpreted to represent an aborted necking domain. Thinning west of the GB defines a necking domain that transitions into the hyperthinned domain of the DGM. A ridge of serpentized mantle reaches the seafloor in the DGM (ODP Site 637, km 10) (Boillot et al. 1987). To adjust the relative gravity high at the GIB the Moho has been modeled as rising to a depth of 16 km, under a thick (> 6 km) depocenter. Refraction and reflection seismic data indicate a crustal thickening to the west of the GIB (Pérez-Gussinyé et al. 2003) reaching 18 km thickness and typical continental crust density values (2.72 g/cm^3). To fit the Bouguer anomaly minimum values observed west of the GB (130–140 km from the western end of the section) it has been necessary to assume a lower density upper continental crust (2.65 g/cm^3). This change in upper crust density coincides with a thinning of the lower continental crust westwards.

To fit the Bouguer anomaly maximum at the DGM (25–65 km from the western end of the section) the Moho

has been modeled as rising to a depth of 9 km (Lymer et al. 2019) and it has been included an undifferentiated crust block (2.6 g/cm^3) resting on it.

Transverse Gravity Model 2 (TGM2) (Fig. 5)

This model is composed of two sections (TGM2A and TGM2B) whose ends are offset by 15 km in the N-S direction: TGM2A is located in the Iberian Abyssal Plain (IAP) and TGM2B is its continuation into the Peniche Basin (Figs. 1, 3 and 5). This model is supported by MCS profiles that were used to constrain crustal basement thickness and Moho depths: Lusigal 12 (Beslier 1996) and its TGS extension (see Sutra et al. 2013) and also by ODP Legs 149 (Sawyer et al. 1994) and 173 (Whitmarsh et al. 1998). ODP Sites 899, 1065, 1069 and 1070 lie in the proximity of the section. The shallow structure follows the interpretation of Amigo-Marx et al. (2019) and is constrained by well data, and MCS data from Portugal Deep 2000 survey by TGS-NOPEC PD00 (PD00-902, PD00-117), line ISE11 and a vintage seismic line (SH74-832). The Moho's first approximation has been modified from Díaz et al. (2016). The base of the crust along this section was constrained by reflection data of the IAM9 profile (Dean et al. 2000).

The main feature in TGM2 is that the proximal domain is broader than in TGM1 and that thinning of the continental crust occurs over 200 km. A ridge of serpentized mantle reaches the seafloor in the IAP (ODP Site 900, km 15, lies close to a north to south transition from thinned continental crust to what is interpreted as basement of mainly serpentized peridotite; Dean et al. 2000).

To adjust the BA values in the proximal to necking domain transition while honoring the Moho depth proposed by Díaz et al. (2016), thick (> 6 km) depocenters, not completely evident on MCS, have been modeled. To fit the increment of BA values observed under the Peniche Basin (140–160 km from the western end of section TGM2B, in the necking domain) it has been necessary to assume a lower density upper continental crust (2.65 g/cm^3). Refraction and reflection seismic data indicate a crustal thickening to the west of the Peniche Basin (similar to Sutra et al. 2013) reaching 18 km thickness and typical continental crust density values (2.7 g/cm^3). The change in upper crust density coincides with a thinning of the lower continental crust westwards. Along the western section (TGM2A), a serpentized mantle has been modeled along its entire length, that consists of a highly serpentized mantle unit (from 2.7 to 2.85 g/cm^3) and a medium serpentized mantle unit (3 g/cm^3).

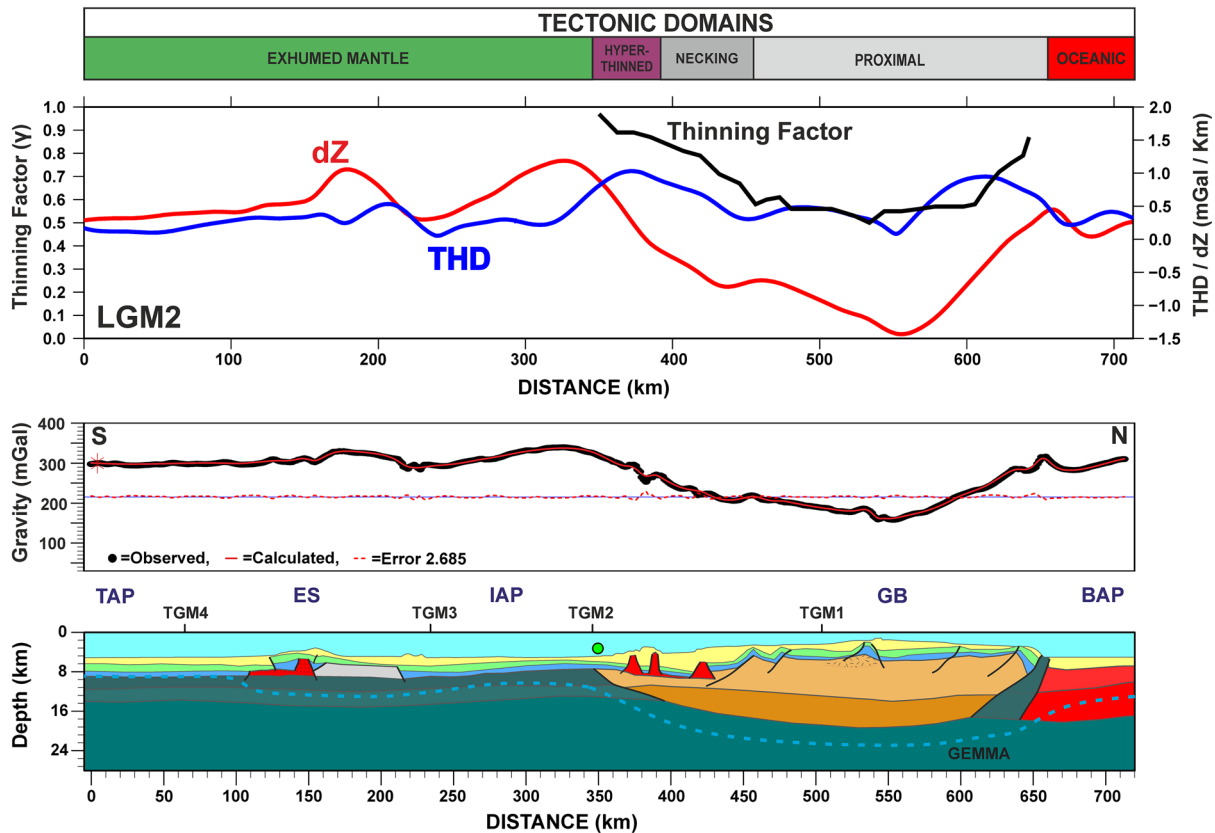
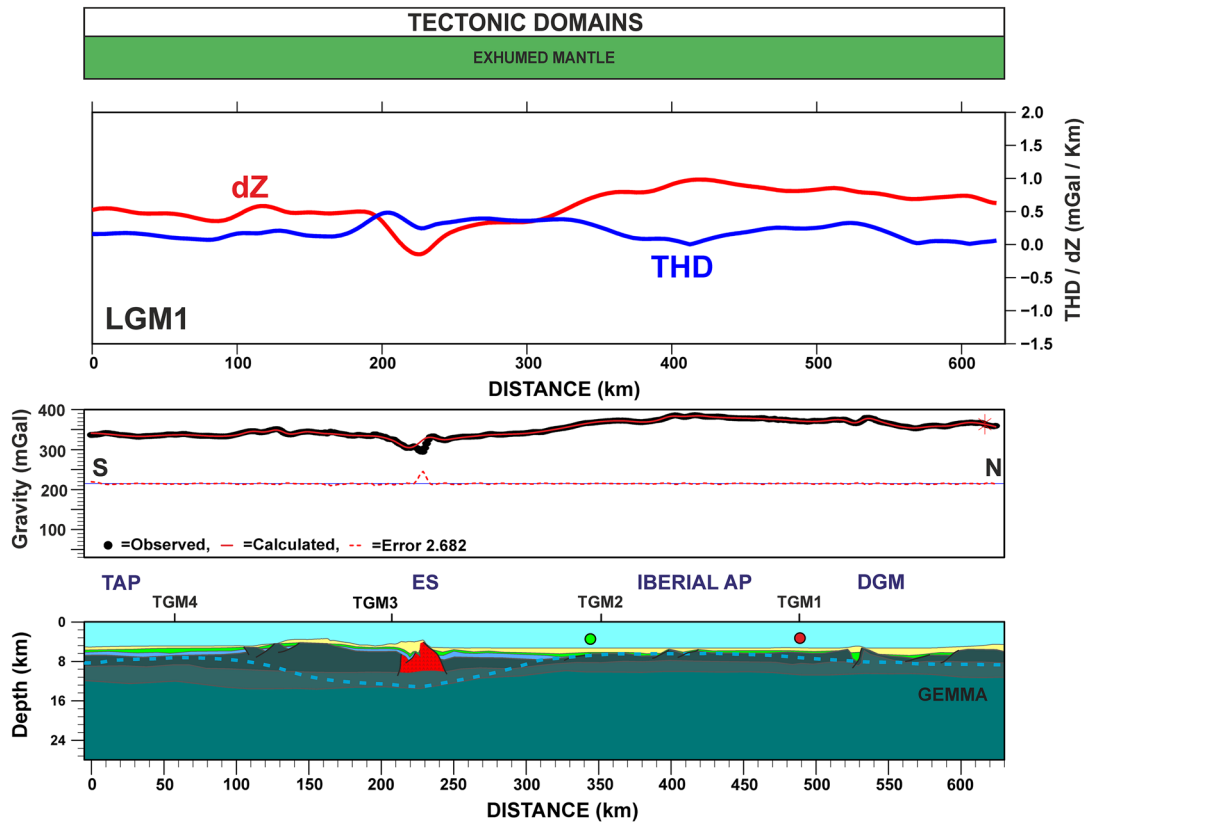


Fig. 7 Adjusted Longitudinal Gravity models LGM1 and LGM2 (see location on Figs. 1 and 3). Moho surface GEMMA (Reguzzoni and Sampietro 2015) is plotted over the gravity model (dashed coloured line). Above the models: Plot of calculated Thinning Factor (γ), Total Horizontal (THD) and Vertical (dZ) derivatives of Bouguer anomaly along the sections. Top: Proposed Tectonic domains distribution. *DGM* Deep Galicia Margin; *BAP* Biscay abyssal plain; *GB* Galicia Bank; *IAP* Iberian abyssal plain; *TAP* Tagus abyssal plain; *ES* Estremadura Spur. (See text for the explanation)

Transversal Gravity Model 3 (TGM3) (Fig. 6)

This model is a 390 km long W-E section that starts in the Tore Rise, crosses the Peniche Basin and the adjacent Lusitanian Basin (Figs. 1 and 6). The easternmost portion of this section is coincident with the model proposed by Sánchez de la Muela et al. (2015). The model is supported by a TGS-Nowec reflection seismic profile integrated into a 2D gravity database of Austin Exploration. These authors defined the pre-salt mega-sequence and the evaporitic units. The density of each unit has been obtained by correlation with refraction seismic velocities (Krawczyk et al. 1996; Dean et al. 2000; Druet et al. 2018).

As opposed to TGM1 and TGM2, this section displays a much narrower necking domain: the proximal domain is 55 km wide, and transitions into a roughly 30 km wide necking domain that gives way to an extremely broad hyperextended domain (hyperthinned and exhumed mantle domains) to the west from 280 km.

The proximal domain is characterized by the presence of thick depocenters in several grabens and half-grabens controlled by normal faults. Further west, in the Peniche Basin, the depocenter located between km 315 and 345 matches well with the G Basin defined by Alves et al. (2006), with up to 8.5 km of sedimentary infilling. To adjust the increase in BA across the Peniche Basin, the Moho has been modeled at a shallower depth (16 km), than in the GEMMA model. It has also been necessary to assume a higher density upper crust to the west (2.75 g/cm^3 , as opposed to 2.65 g/cm^3). The change in upper crust density coincides with a thinning of the lower continental crust westwards.

Transversal Gravity Model 4 (TGM4) (Fig. 6)

This is a 345 km long W-E section that begins close to the Madeira-Tore Rise, crossing the TAP and adjacent Alentejo Basin (Figs. 1 and 6). It is supported by multi-channel seismic-reflection line IAM-5 (Banda et al. 1995) and the deep structure is constrained with seismic velocity models from Afilhado et al. (2008).

As in the case of TGM3, the continental crust thins very rapidly, with the transition between the proximal domain and exhumed mantle domain occurring in only 80 km. However, the thickness of depocenters in the proximal and

necking domains is smaller than those in the TGM3 model. The model shows a proximal domain 40 km wide that transitions across a 25 km wide necking domain into a very broad hyperextended domain (hyperthinned and exhumed mantle domains). To adjust Bouguer anomaly local maxima under the TAP (km 235–255), interpreted to be upper crust extensional allochthons, it has been necessary to increase the continental crust density (from 2.75 to 2.8 g/cm^3). Finally, the beginning of the oceanic crust does not present a significant gravimetric signal, but it has been established from the presence of magnetic isochrone M3 (Fig. 3b).

Longitudinal gravity models

Longitudinal gravity models present two types of large-scale structure (Figs. 7 and 8). On the one hand, the more distal section (LGM1) extends through the exhumed mantle domain, highlighting only variations in the thickness of the serpentinized mantle units (thicker in the southern half), some igneous intrusive bodies (Miranda et al. 2010; Pereira et al. 2017) and variations in the, generally low, thickness of the Mesozoic-Cenozoic cover thickness. On the other hand, the general structure of LGM2, LGM3 and LGM4 consists of a thick continental crust in the north (proximal and necking domains) and a hyperextended domain (hyperthinned or exhumed mantle domain) in the south (as already observed by Pickup et al. 1996; Dean et al. 2000). The northern, thick continental crust has a sharp northward transition to an area of oceanic crust across a zone of tectonic inversion (Druet et al. 2018).

The models are constrained in their northern half by ISE-1 seismic refraction data (Zelt et al. 2003) and by the reflection and refraction seismic profile ISE-9 (Clark et al. 2007). The southern half is constrained by the IAM-5 deep seismic profile (Afilhado et al. 2008). The GEMMA Moho depth model (Reguzzoni and Sampietro 2015) has been also used as a first approximation along these sections.

Longitudinal Gravity Model 1 (LGM1) (Fig. 7)

The LGM1 starts in the TAP, northwest of the Gorringer Bank, crosses the Madeira-Tore Rise, the IAP, transects the DGM and ends up north of it (Figs. 1 and 7).

The entire section runs along the exhumed mantle domain of the WIM. The exhumed mantle is serpentinized, as indicated by ODP wells 1070 and 637, and two layers of varying serpentinization have been distinguished based on the gravity signal (upper unit from 2.8 to 2.85 g/cm^3 ; lower unit 3 g/cm^3). The thickness of serpentinized mantle is greatest in the south than in the north, with the sharpest change in thickness occurring across the Tore Seamount. The Bouguer anomaly low across the Tore Rise is accounted for by the igneous nature (probably basic or ultra-basic) of the Tore Seamount,

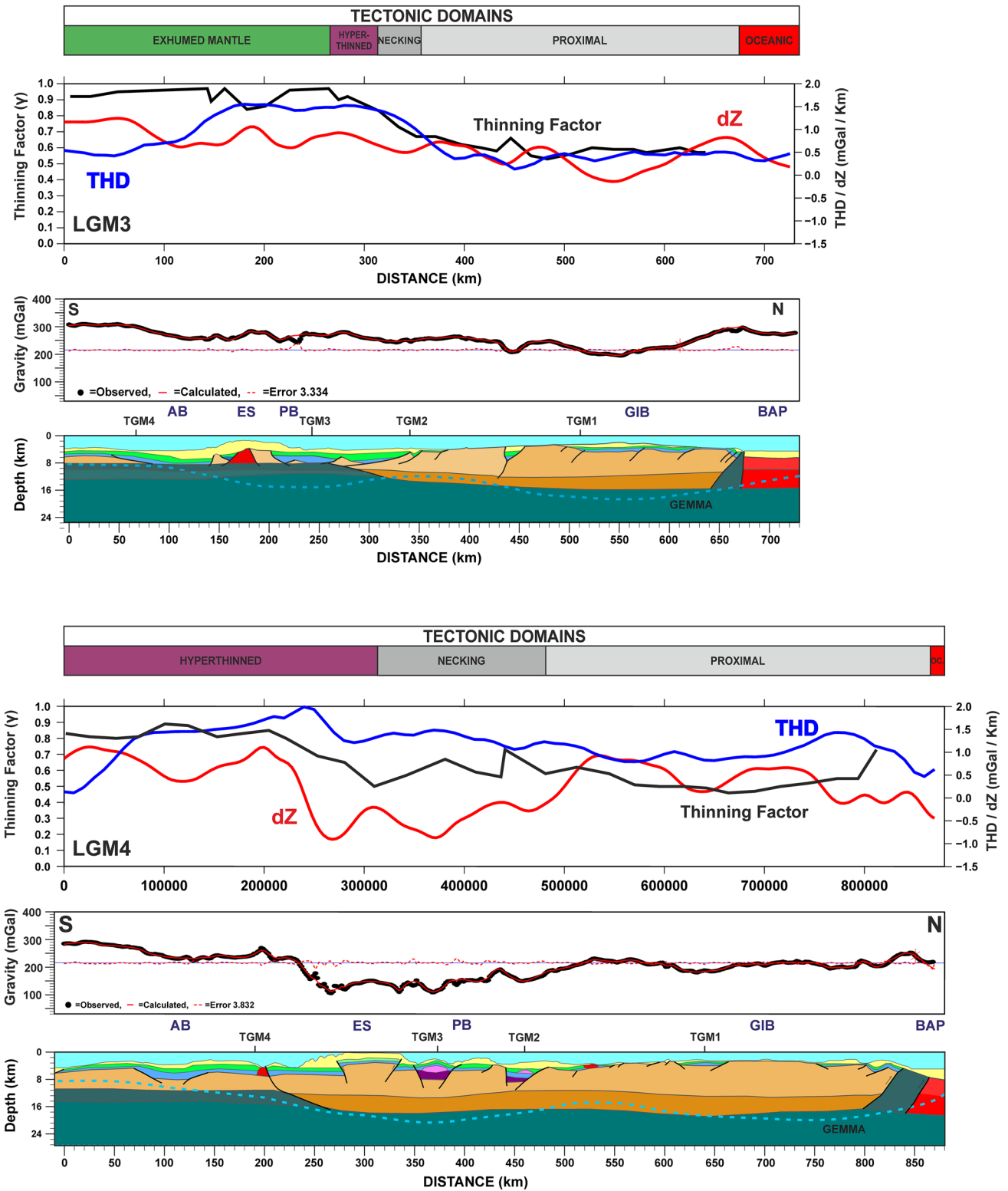


Fig. 8 Adjusted Longitudinal Gravity models LGM3 and LGM4 (see location on Figs. 1 and 3). Moho surface GEMMA (Reguzzoni and Sampietro 2015) is plotted over the gravity model (dashed coloured line). Above the models: Plot of calculated Thinning Factor (γ), Total Horizontal (THD) and Vertical (dZ) derivatives of Bouguer anomaly

along the sections. Top: Proposed Tectonic domains distribution. BAP Biscay abyssal plain; GIB Galicia Interior Basin; PB Peniche basin; AB Alentejo basin; ES Estremadura Spur. (See text for the explanation)

as suggested by the magnetic data and observations made by Miranda et al. (2010). In the northern part of the model, high Bouguer anomaly values (300–400 mGal) are adjusted by means of a thinning of the serpentinized mantle unit and the rising of the unaltered Mantle.

Longitudinal Gravity Model 2 (LGM2) (Fig. 7)

This gravity model (Figs. 1 and 7) starts in the TAP, north the Gorringe Bank, crosses the IAP, transects the east of Galicia bank and finishes in the Biscay Abyssal Plain (BAP). The model is constrained in its northern half by model GM6 of Druet et al. (2018). This section transitions from an exhumed mantle domain in the TAP and IAP, in the south, to an area of relatively thick continental crust in the GB in the north. In its northern end the section enters the oceanic domain of the Bay of Biscay.

As with LGM1, basement in the southern exhumed mantle domain is interpreted to consist of a 2-layered serpentinized mantle (upper unit from 2.9 g/cm³; lower unit 3 g/cm³). This domain is punctuated by a positive gravity anomaly interpreted to be caused by roughly 100 km of undifferentiated thinned crust (density = 2.6 g/cm³ and 2.5 km thick) and an adjacent igneous body (as suggested by magnetic data). This crustal block correlates well with the western prolongation of the Estremadura Spur. The southern limit of this block fits well with a reverse-type contact, possibly with a Cenozoic sedimentary depocenter close to this limit.

In the Northern part of the section the transition from the exhumed mantle domain to the continental crust occurs at km 345, by means of a north-dipping contact. This thickening and change of crustal properties are well marked by a strong gravity gradient. In order to hold the Moho depth proposed by Clark et al. (2007), it is necessary to model a relatively thicker lower continental crust unit.

A series of short-wavelengths gravity highs are observed between 365 and 435 km, with also high frequency strong magnetic anomalies, that have been modeled as high-density basement bodies. From the thickest crust zone (km 550) the Bouguer anomaly rises sharply northwards with two short-wavelength and great amplitude gravity highs. To adjust these data it is necessary to model a reverse contact between the continental and oceanic crusts and a narrow ocean-continent transition. This solution is similar to that proposed by Druet et al. (2018). The reverse nature of the contact is supported by the downward flexure of the oceanic crust and presence of a depocenter in the footwall, as indicated by the relative gravity low.

Longitudinal Gravity Model 3 (LGM3) (Fig. 8)

This gravity model starts in the Alentejo Basin, crosses the Peniche Basin and the GIB, and finishes in the Biscay

Abyssal Plain (Figs. 1 and 8). The structure of this profile is very similar to that observed on LGM2 and has been adjusted with similar criteria. This section transitions from an exhumed mantle domain in the Alentejo Basin and the southern part of the Peniche Basin, to an area of relatively thick continental crust in the GIB in the north. In its northern end the section enters the oceanic domain of the Biscay Abyssal Plain.

As with previous models, basement in the southern exhumed mantle domain is interpreted to consist of a 2-layered serpentinized mantle (upper unit 2.9 g/cm³; lower unit 3.1 g/cm³). This domain is punctuated by two positive gravity anomalies interpreted to be caused by roughly 70 km of undifferentiated thinned crust each one, first one at the Alentejo Basin (density = 2.75 g/cm³ and 2.5 km thick), the second one (density = 2.65 g/cm³ and 4.5 km thick), and an adjacent igneous body (as suggested by magnetic data, Fig. 3b). This last crustal block correlates well with the prolongation of the Estremadura Spur. The southern limit of this block fits well with a reverse-type contact, possibly with a Cenozoic sedimentary depocenter close to this limit.

In the Northern part of the section the transition between the exhumed mantle domain and the continental crust occurs at km 260, by means of a south-dipping contact. This thickening and change of crustal properties are well marked by a steeped gravity gradient. It is necessary to model a relatively thicker lower continental crust unit (2.65 g/cm³), faulted and tilted to the south. The thickening of the continental crust generates a gravity gradient reaching higher values in the area of maximum crustal thickening (km 550). This gradient is accompanied by a change in crustal density (2.75 g/cm³) and a thicker lower continental crust along the GIB (km 440). From the thickest crust zone (500–550 km) the Bouguer anomaly rises sharply northwards with two short-wavelength and great amplitude gravity highs. To adjust this anomaly, it is necessary to model a reverse contact between the continental and oceanic crusts and a narrow ocean-continent transition. This solution is similar to that proposed for LGM3.

Longitudinal Gravity Model 4 (LGM4) (Fig. 8)

This 870 km length section is the closest to the western Iberian continental shelf. It starts in the Alentejo Basin, crosses the Peniche Basin, transects the GIB, and finishes in the Biscay Abyssal Plain (Figs. 1 and 8).

The southern part of the section corresponds to the hyperthinned domain. It transitions north into a domain of thicker continental crust (necking domain) in the vicinity of the Estremadura Spur. At its northern end, it enters into the oceanic domain of the Biscay Abyssal Plain.

Local gravity lows in the Alentejo and Peniche Basins correlate with sedimentary depocenters. In the between both

basins, a sharp gravity high located near km 200 has been adjusted by interpreting the presence of an igneous body, as suggested by magnetic data. This body also coincides with the transition from the hyperthinned into the necking domain that underlies the Peniche Basin and GIB. Further north, near km 300, a major popped-up block of continental crust corresponds to the Estremadura Spur, North of the Peniche Basin, the continental crust becomes thicker under the GIB, with limited depocenter thickness on this section. As with the previous models, the northern limit of the WIM is interpreted to be a reverse contact placing the WIM unit over oceanic crust at the Biscay Abyssal Plain.

Discussion

Relationships between Tectonic Domains and Gravity data

The values of BA, THD and Dz obtained from our modelling have been compared with the conceptual section of Tugend et al. (2014) and Cadenas et al. (2018), (Figs. 2a and 9) by calculating its gravimetric signal, assigning densities based

on the WIM refraction seismic data. The model results are displayed in Fig. 10, right panel.

This conceptual section allows us to compare the Bouguer anomaly value and the crustal thinning factor in the different domains. The values of the gradients have been calculated on a 2D model, so their absolute values are not directly comparable to the data of the actual gradients obtained from the Bouguer Anomaly grid (3D).

In Fig. 10, left panel we have plotted the values of BA (A), THD (C) and dZ (D) for all of the transverse models presented above, along with the magnitude of crustal thinning (B). The values plotted correspond to 5–10 km sampling intervals along the adjusted gravity models and classified depending on the structural domain defined along the sections. For each domain, the values are represented in a box-plot graph (Fig. 10, left panel) and summarized in Table 2.

BA, THD and dZ show significant variations in their absolute values along the margin, but clear patterns emerge:

- (A) The BA clearly reflects the thinning of the continental crust and gradual mantle shallowing (e.g., Cowie et al. 2015; Stanton et al. 2016; Druet et al. 2018) and

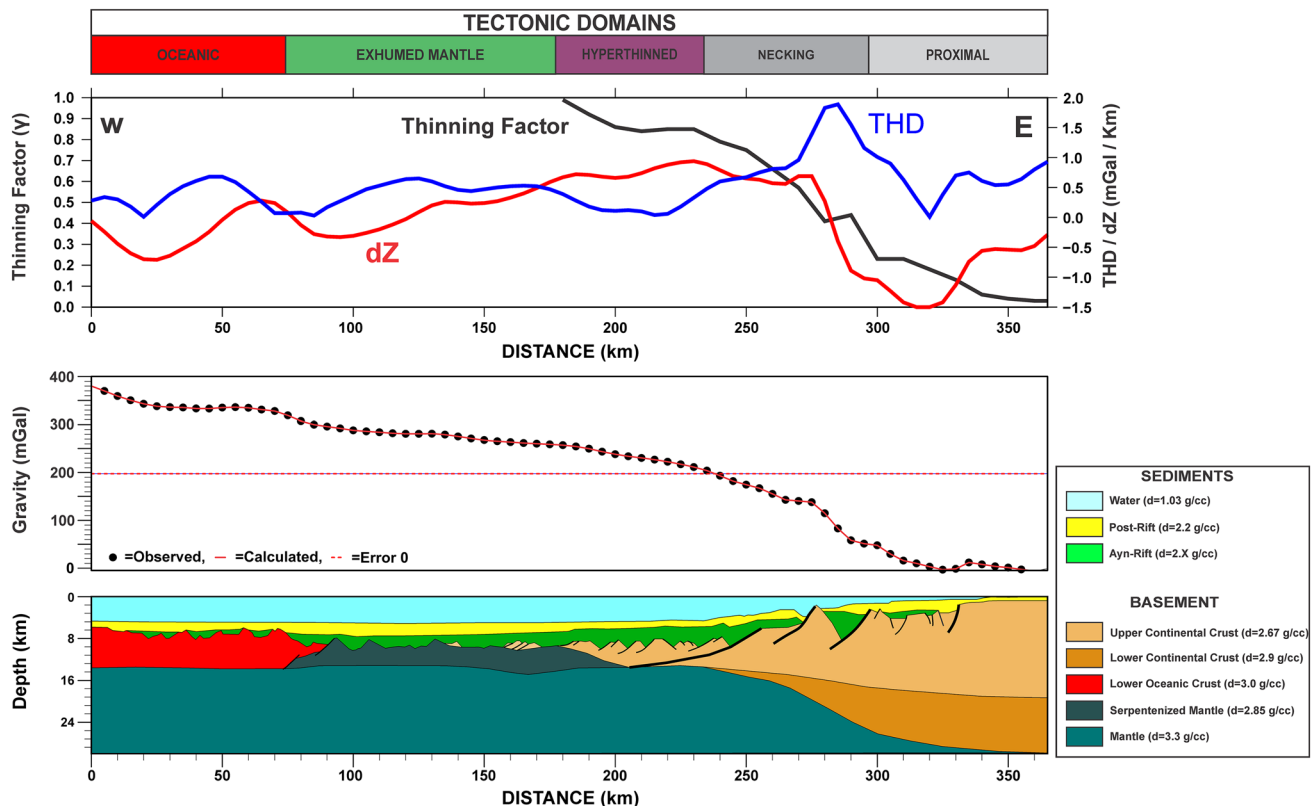


Fig. 9 Adjusted Theoretical Gravity model based on Tugend et al. (2015) and Cadenas et al. (2018), with the distribution of conceptual tectonic domains. Density values has been assigned following velocity/density empirical correlations (Table 1). Above the model: Plot of

calculated Thinning Factor (γ), Total Horizontal (THD) and Vertical (dZ) derivatives of Bouguer anomaly along the sections (See text for the explanation)

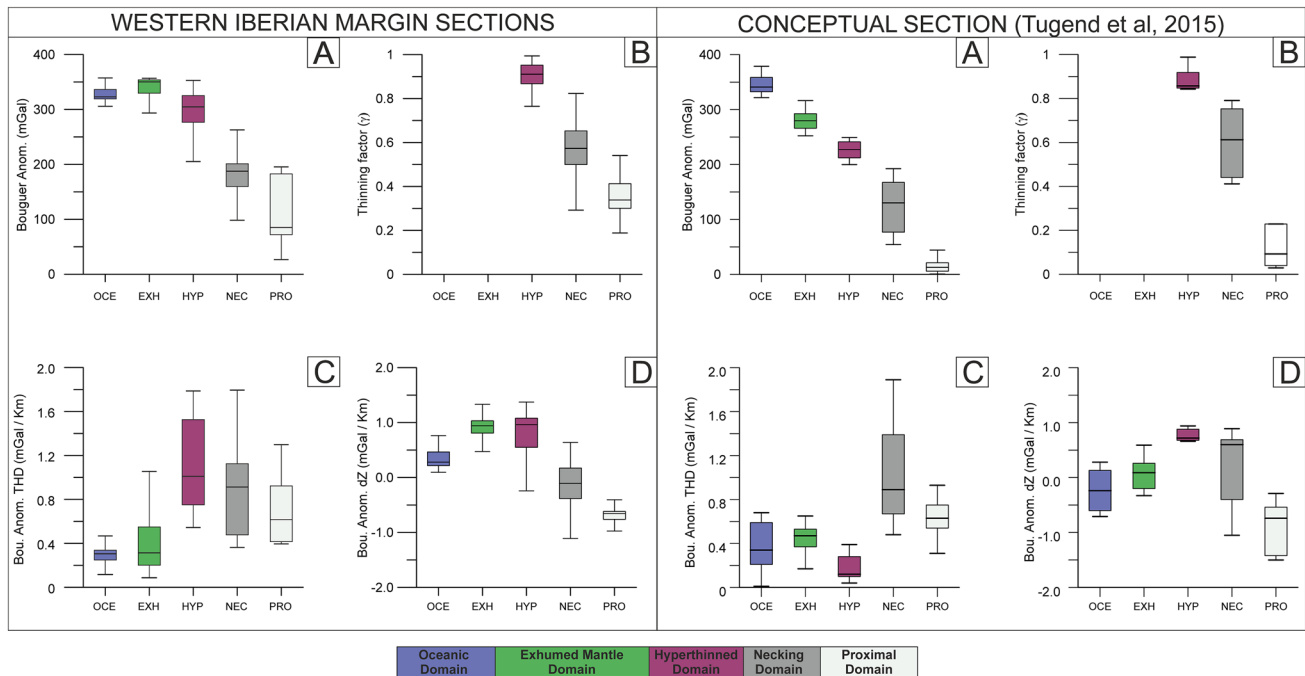


Fig. 10 Left panel: Box-plot distribution of **a** Bouguer anomaly, **b** Thinning Factor (γ), **c** Bouguer anomaly THD and **d** Bouguer anomaly dZ values along the transverse models (GMT1 to GMT4). Right panel: The same parameters calculated along the conceptual

model shown in Fig. 9. Note the closed correlation between Bouguer Anomaly and Thinning factor (γ) and that necking and Hyper-thinned domains are defined by high THD values of BA (see text for explanation)

Table 2 Resumed values for the four parameters (Bouguer anomaly, Thinning Factor, THD and dZ) calculated along the lithospheric sections shown in Fig. 11

Tectonic domains	Oceanic (min/max)	Exhumed mantle (min/max)	Hyper-thinned (min/max)	Necking (min/max)	Proximal (min/max)
Bouguer anomaly (mGal)	305/355	295/355	205/350	100/260	25/195
Thinning factor (γ)	–	–	0.75/1	0.3/0.82	0.2/0.55
Bouguer anomaly ThD (mGal/km)	0.11/0.5	0.09/1.05	0.5/1.8	0.4/1.8	0.4/1.3
Bouguer anomaly DZ (mGal/km)	0.1/0.75	0.5/1.3	0.25/1.4	(– 1.1)/0.7	(– 1)/(– 0.4)

this increase correlates well with the trend in thinning factor. The exhumed mantle and oceanic domains are difficult to differentiate as both have positive and stable values of BA (> 300 mGal).

- (B) BA THD values in turn reveal an increase in magnitude from the proximal to the hyperthinned domain. Maximum values in the hyperthinned domain decrease oceanward rapidly, with the exhumed mantle and oceanic domains displaying THD values lower than all the other domains.
- (C) Finally, BA dZ values display a maximum in the hyperextended domain (hyperthinned and exhumed mantle), with lower, positive, values in the oceanic domain and with null to negative magnitudes in the necking and proximal domains.

These results indicate that the combination of BA, THD and dZ can be used, together with seismic sections and ODP wells, to identify the transitions between almost all crustal domains of the WIM or even to improve the estimations in regions with no seismic coverage. From ocean to continent: the exhumed domain transitions to the hyperthinned domain at a point of increase in THD and drop in BA; and the hyperthinned domain transitions to the necking domain (the coupling point) at a point of decreasing dZ. The only exception is the boundary between the proximal and necking domains, which is characterized by an increase in all three parameters. Finally, to more precisely define the beginning of the oceanic domain to the west, the position of the first significant magnetic anomaly has been used as an additional indicator (see “Discussion” section below).

Trends in BA (A), THD (C) and dZ (D) from the conceptual section (Fig. 10, right panel) deviate significantly from our own results, but so does the overall interpretation of the margin.

Other authors have used the sections previously published by Zelt et al. (2003) and Sutra et al. (2013), at the NW of the Iberia margin, to construct crustal-scale models, using the same type of data, identifying boundaries between tectonic domains:

The results of magnetic and gravity forward modeling published by Stanton et al. (2016) are very similar to the TGM1 and TGM2 gravity models presented in this work, but it differs in the criteria of distribution of tectonic domains along those sections. The major difference lies in the location of the landward limit of the necking domain and its boundary with the distal domain. The definition of these boundaries is more accurate with the use of total horizontal (THD) and vertical gradients (dZ) of Bouguer anomaly as additional indicators. The final results of the work presented by Stanton et al. (2016) show a comparison between the distribution of domains over the sections based on the seismic and ODP observations and the domain's boundaries derived from the interpretation of the gravimetric and magnetic anomaly maps.

The major differences between the forward modeling made by Cowie et al. (2015) over the ISE 1 and LG12-TGS seismic sections and our models lie in the geometry of the Moho (calculated by gravimetric inversion) and the distribution of tectonic domains along those sections. The main difference lies in the location of the oceanward boundary of the necking domain. To identify the boundary between the crustal necking zone and hyperextended crust they used a combination of changes in crustal basement thickness, variations in residual depth anomaly (RDA) and changes in continental lithosphere thinning factors.

The present study provides criteria to identify tectonic domains from the results obtained from the gravity modeling of the seismic sections, and the observations made in the maps of AB, THD and Dz.

A similar approach to defining crustal domains based on gravity gradients was used in another Atlantic passive margin by Fernandez et al. (2020). In their case, the patterns observed were different to those presented here. Whereas the THD in the WIM reaches a maximum in the hyperthinned domain, the THD in the southwestern African passive margin displays two distinct maxima: one along the necking domain and one along the distal to oceanic domain transition (Fernandez et al. 2020). The difference in gravimetric signal for both margins is yet to be explored. One possible cause, however, is the fact that the southwestern African margin contains a significant amount of magmatic additions and limited or no mantle exhumation (Fernandez et al. 2020) whereas the WIM is magma-poor with broad areas of mantle

exhumation. The presence of salt is definitely a big difference. There are examples in Kwanza Basin (Lavie et al. 2019; Fernández et al. 2020) where a step in the basement is observed associated to the transition from continental crust. This step can be explained by the volcanic addition at break-up time. Fernández et al. (2020) suggested that volcanism continues during the precipitation of Ezanga-Loeme evaporites, which act as a buttress, creating the step. In the case of Iberia, the absence of salt may facilitate the opening of the oceanic domain, showing a smoothing transition.

Another case of 2-D forward gravity modeling is the work made by Dragoi-Stavar and Hall (2009) to examine changes in crustal structure of conjugate portions of the South Atlantic volcanic margins. Models were constrained with available seismic data, and geologic information. Correspondence between residual anomalies and deep structure suggested that changes in gradient may be used to approximately delineate crustal domain boundaries.

The modelling results of the NE Atlantic made by Haase et al. (2016), together with the tilt derivative gravity, is another example of the used of these techniques to better understand the location of the continent-ocean boundary.

This type of analysis might fail in those areas where a limited amount of constraints are available. For instance, in salt passive margins like Angola or Brazil, it is necessary to understand the nature and behavior of the salt. It is assumed that the average salt density is 2.18 g/cm^3 , however, a detailed study in these areas reveals a huge range, based on its chemical composition. Following with the Angola margin (Fernández et al. 2020) demonstrated the presence of volcanic bodies and show its lateral extension but was necessary an intense drilling campaign before to recognize them. In the same way, the presence of large carbonate platforms (i.e. South China Sea) can alter the modeling. At crustal-scale, refraction profiles can recognize high-velocity areas.

Proposed Tectonic Domains along the WIM

Given the relationships between the gravity data and the tectonic domains described above, we have mapped the thinning factor (Fig. 11) and the tectonic domains along the margin, constrained along the eight calibrated sections (Fig. 12). A comparison with the definitions proposed by previous authors is shown in Fig. 13.

Two sectors of the WIM are clearly differentiated (Fig. 12):

- (A) In the north, the extensional structure is more complex, with two necking domains, at the GIB and at the DGM. This suggests the presence of two rift branches: one aborted rift (GIB) and the one further west (Murillas et al. 1990; Manatschal and Bernoulli 1999; Druet et al. 2018), whose evolution led to Atlantic oceanic crust

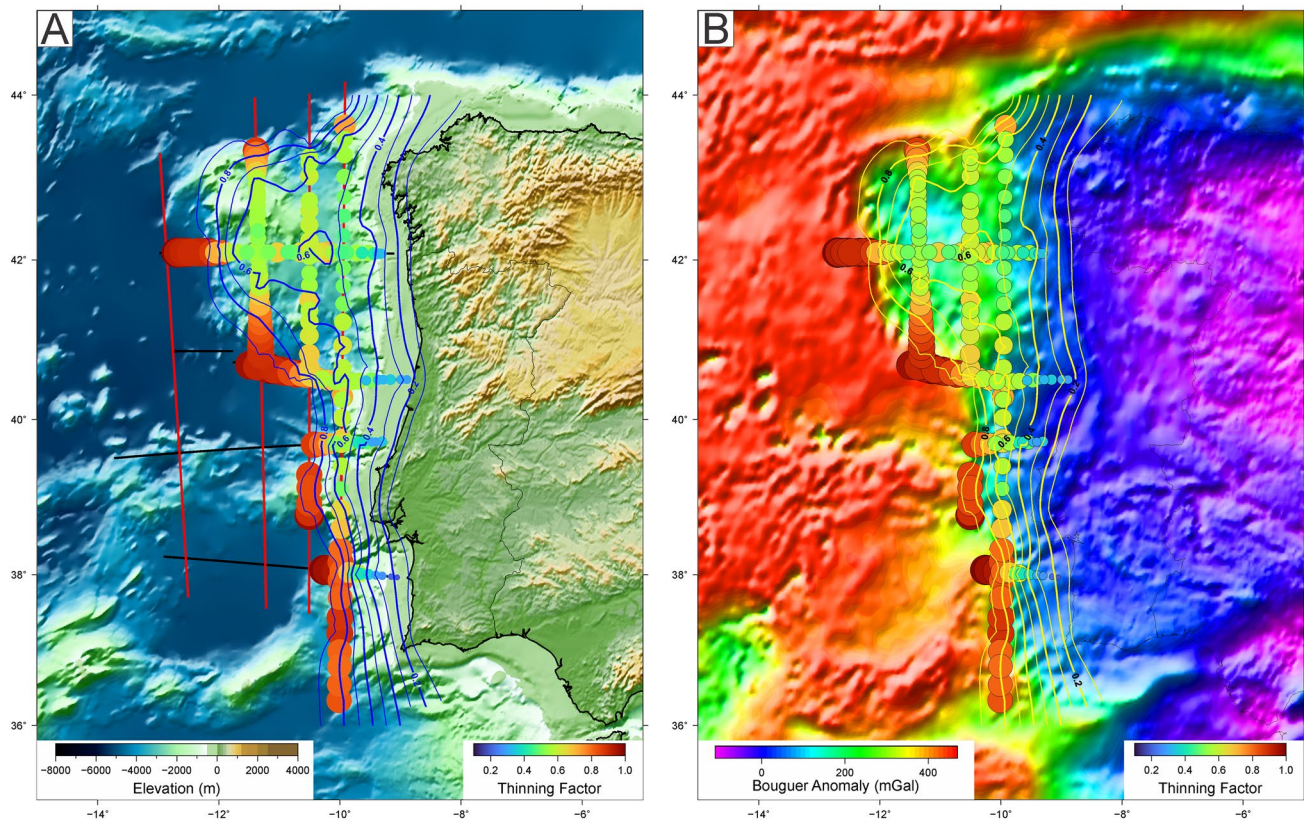


Fig. 11 Thinning factor (γ) represented by proportional circles colored by γ value and contour each 0.1 of this factor calculated from the continental crustal thickness calibrated along the eight litho-

spheric sections. The values are represented over the elevation map (a) and on the Bouguer Anomaly map (b) (see text for explanation)

formation. This complex extensional pattern is associated with a narrower exhumed mantle domain when compared to the south WIM. The outer necking zone merges southwards with the eastern one (the GIB) following a NW–SE orientation.

- (B) The southern sector is characterized by a narrower continental domain (proximal, necking and hyperthinned), (Manatschal et al. 2015; Stanton et al. 2016) with thinning of the continental crust occurring in a much narrower band and juxtaposed with a very broad exhumed mantle domain.

The limit between the northern and southern sectors follows then a NW–SE orientation that can be observed clearly on the Bouguer anomaly gradient maps (THD and dZ) (Fig. 12b and c). This limit has the same trend that the main Variscan fabric presents in the onshore continental crust.

The NW–SE orientation of the limit between the north and south sectors looks quite sharp, similarly to the other segments that are offset by transversal transfer zones in the south. We consider that our maps suggest similar, unrecognized yet, transfer structures existing at the transition between the two sectors to explain this transition;

not only because it follows the trend of Variscan fabric but the radical change in the width of the crustal domains northern and southern of this feature, the drastic reduction in the continental crust thickness to the SW of the GB, with a necking zone (that may not be just a necking zone, but rather a combination of extensional deformation and a transfer zone) with NW–SE orientation. A similar transfer zone SW of the GB is been suggested in previous work by Pinheiro et al. (1992) and Whitmarsh et al. (1993) based primarily on the analysis of magnetic anomalies.

There is a similar lineament in the distal domain facing the TF (Fig. 12a–c) that coincides with another possible transfer zone at the TAP, also suggested by Pinheiro et al. (1992) and Whitmarsh et al. (1993)

The transfer zones highlight on this work (Figs. 12 and 13) separate the three segments into which the WIM is classically divided, from south to north: Tagus Abyssal Plain sector, South Iberia Abyssal Plain sector and West Galicia Margin sector. This segmentation is due to the succession of different extensional pulses, Late Jurassic (~150 M.a.) to Early Cretaceous times (~120 M.a.) (e.g. Murillas et al. 1990).

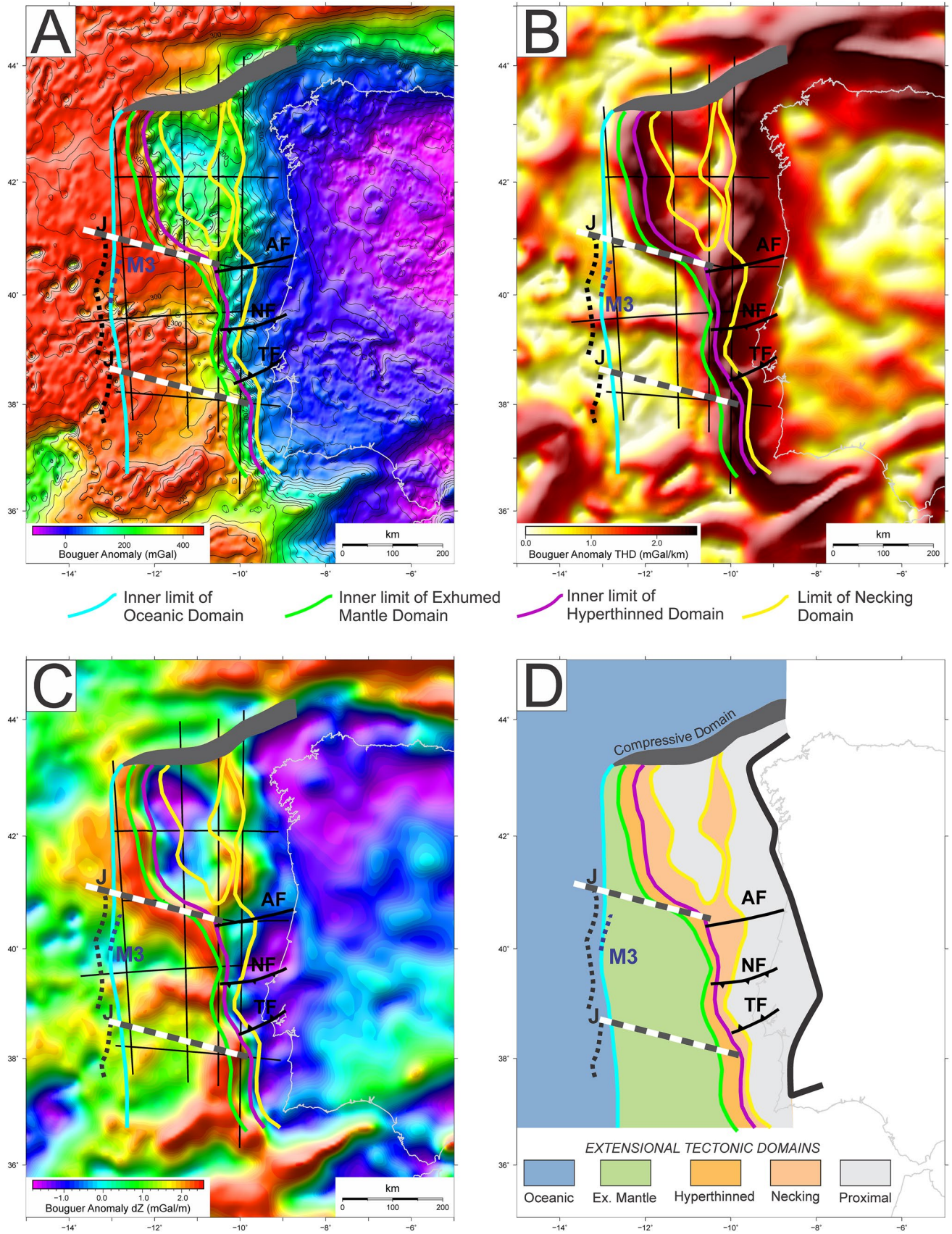


Fig. 12 Proposed Tectonic Domains distribution for the Wester Iberian Margin over **a** Bouguer anomaly, **b** Bouguer anomaly Total Horizontal Derivative, **c** Bouguer anomaly vertical derivative. J anomaly and M3 isochrone are also plotted in the maps. The limits between domains have been defined along the eight lithospheric sections and mapped following gravity signal (see text for explanation). The white and grey dash lines are possible transfer zones. *TF* Tagus Fault; *NF* Nazare Fault; *AF* Aveiro Fault

Several oblique structures, both extensional and inversion-related, are superimposed on this general pattern. These structures, especially visible in the longitudinal gravity models, displace the crustal domains laterally (e.g.; Estremadura Spur), or making some extensional domains disappear in the NW of the Iberian margin, where the alpine compressional deformation is more intense (Druet et al. 2018) (the thrust juxtaposing the Galicia Bank on the Biscay Abyssal Plain).

Discussion of proposed Tectonic Domains versus previously defined domains

Figure 13 shows the map with the different tectonic domains proposed in this work and those of previous authors that cover most of the margin.

The boundaries between the previously proposed domains have similar positions in the seismic sections where they have been defined, but they differ according to the criteria used by each author. However, the greatest differences occur in areas where there is no seismic information. It is just in these areas where the positions of the limits of the previous authors clearly differ from the trend of the Bouguer anomaly gradients, which mark density variations with lateral continuity throughout the entire margin.

The Péron-Pinvidic et al. (2013) model (Fig. 13b) assumes a very broad proximal domain along the entire margin, with only a northward opening “embayment” leading to the necking domain over the Galicia Interior Basin. The band of maximum cortical thinning in this model is continued to the N of the Galicia Bank, because these authors do not consider the Cenozoic compressional deformation (e.g., Boillot et al. 1995; Vázquez et al. 2008; Druet et al. 2018), and clearly cuts the areas of maximum values of Bouguer anomaly THD.

The Welford et al. (2010) domains map (Fig. 13c) shows a distribution of the continental crust domain more similar to our proximal zone, although with less extension over the Galicia Bank. The map also shows fluctuations along the limits that do not follow the trends of the Bouguer anomaly gradients. The greatest difference in this map occurs in the south half, where the exhumed mantle domain disappears, and the oceanic domain is directly in contact with the stretched continental crust zone.

The Nirrengarten et al. (2018) domains map (Fig. 13d) shows an oceanward edge of the thinned domain more

similar to our hyperthinned domain at the northern half of the WIM following the trend of the BA THD; but it is broader than ours at the southern half. The exhumed domain is broader than ours at the northern half and slightly narrower at the south of the WIM. The main difference of this model with respect to our map is that they do not differentiate a proximal domain in the north of the WIM and also that they maintain the continuity of the exhumed mantle domain north of the GB. Another difference is that these authors include M3 anomaly in the exhumed mantle domain. The landward limit of the oceanic crust is oceanward (LaLOC) of the J anomaly at the northern segment (Deep Galicia Margin), at the central segment matches approximately the LaLOC; and at the southern segment the LaLOC is continentward of the J anomaly.

In our map, the presence of a compressive domain in the N overridest the necking and hyperthinned domains in the NW of the Iberian Peninsula. The Cenozoic compressional deformation also generates (or reactivates as reverse faults) a series of fragile NE-SO structures in the Estremadura Spur (including the Nazare fault). These faults produce a displacement in the limits of the domains and folds the Bouguer anomaly gradients (Figs. 12 and 13a). These changes in the distribution of the tectonic domains of the extensional margin could not have been detected if the longitudinal sections (N-S) had not been modelled across the margin, which allow the domains to be accurately constrained laterally.

Finally, there is a great difference in the location of the oceanic domain between each of the previously proposed domains cited above due to two factors: (a) the difficulty of delimiting the beginning of the well-defined oceanic crust, and (b) what each author considers by the term “oceanic”.

Because gravity data does not allow discrimination between oceanic crust and exhumed mantle domain, and because the definition of the beginning of the oceanic crust is not a fundamental objective of this work, we have resorted to the use of magnetic data (Fig. 3b) to establish this limit. The most common criteria for defining the beginning of the oceanic crust is the use of the magnetic anomaly that represents the most recent isochrone. However, it should be remembered that serpentinization in the exhumed mantle domain can produce magnetic alignments similar to the expansion characteristics of the ocean floor, with the difference that they are weaker and more variable in intensity (Sibuet et al. 2007). With this in mind, we have used the presence of the first magnetic anomaly representing the most modern isochrone M3-124 My- (Whitmarsh et al. 1990, 1996; Catalán et al. 2013).

Thus M3 anomaly does not clearly demonstrate the existence of oceanic crust, it has been used as a criterion to locate the beginning of the oceanic crust, in the absence of other information.

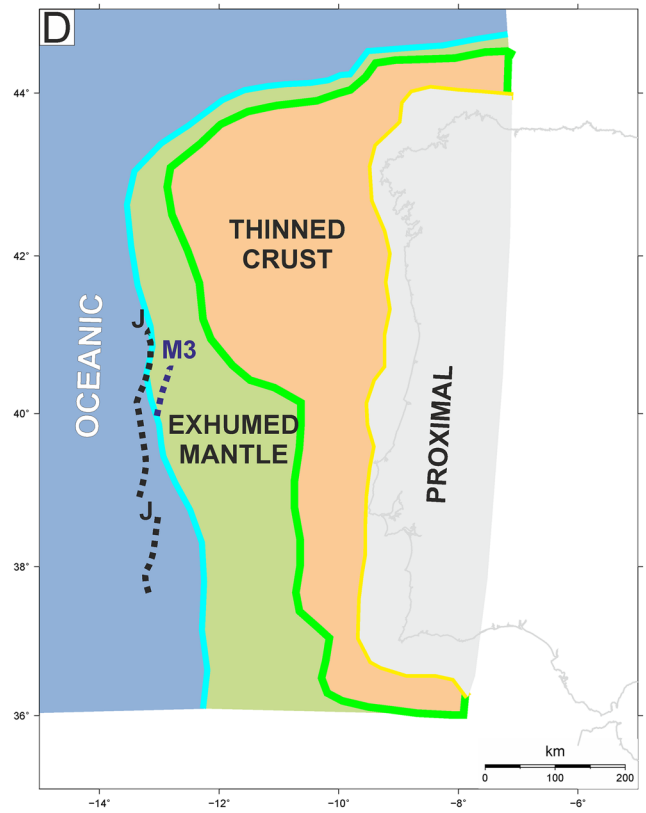
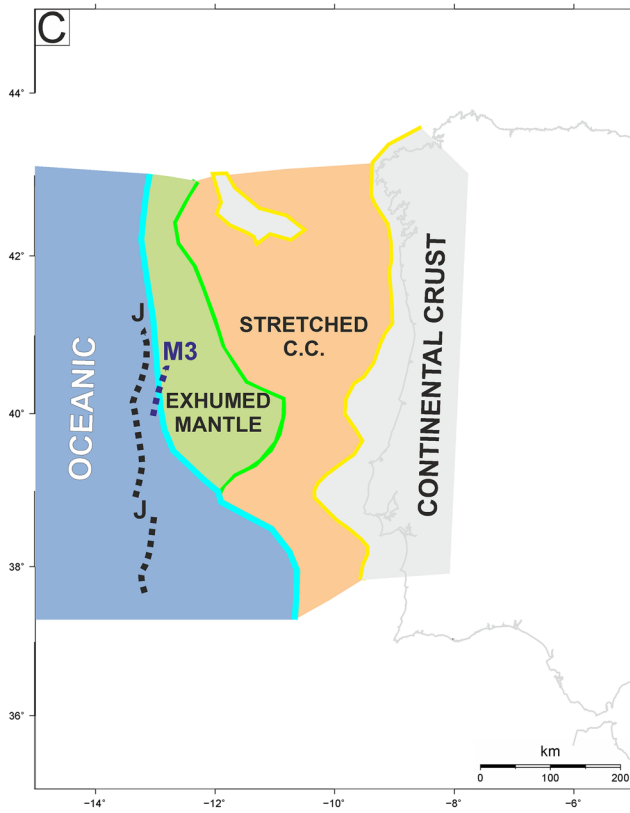
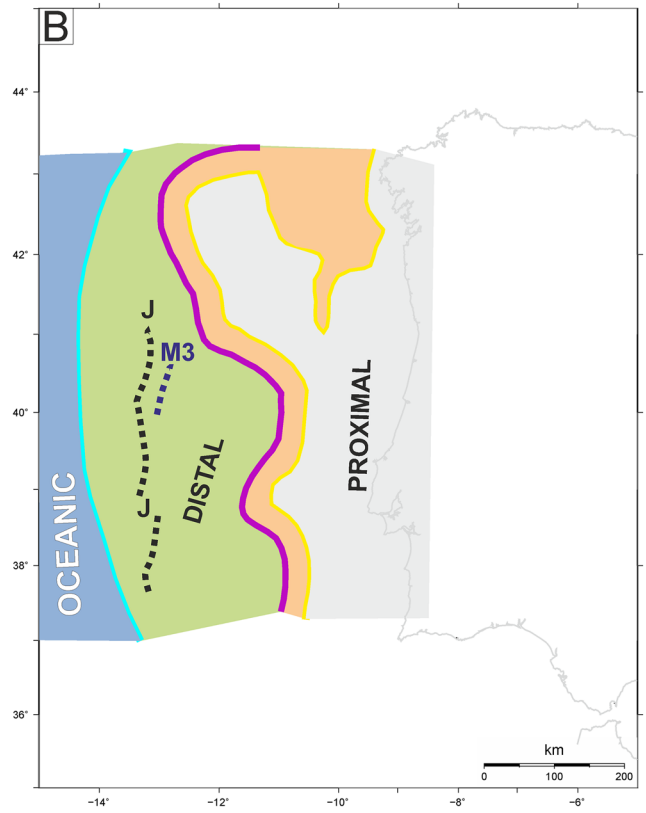
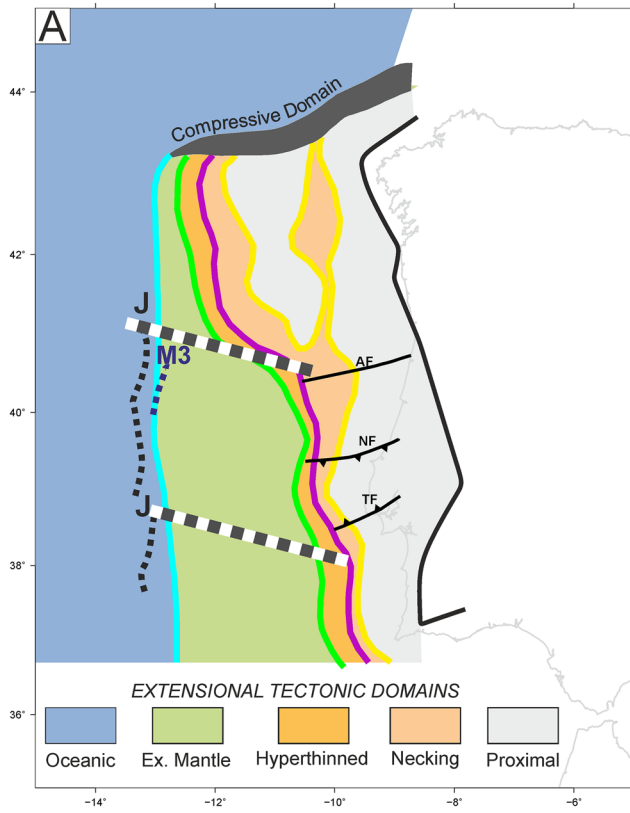


Fig. 13 Tectonic Domains along Western Iberian Margin proposed by: **a** this work, **b** Perón-Pinvidic et al. (2013); **c** Weldfod et al. (2010) and **d** Nirrengarten et al. (2018). Main faults affecting extensional tectonic limits as well as compressive domain are also plotted in our proposed Tectonic Domain map. The white and grey dash lines are possible transfer zones. *TF* Tagus Fault; *NF* Nazare Fault; *AF* Aveiro Fault

In this work, we are proposing a mapping methodology to identify important features of the margin. The structure of passive margins is still debated and the interpretation of these features will vary depending on the dominant paradigm at the time. This technique significantly improves the certainty and accuracy with which passive margin plate tectonic reconstructions can be undertaken according to the methods of Peace et al. (2019) and Nirrengarten et al. (2018), by a better definition and mapping of the Necking line and the oceanward edge of the continental crust. As well as the importance of the location of the necking zone for geodynamic restoration, as the coupling point represent the location where crustal deformation changes to coupled that leads to the onset of mantle.

Conclusions

The aim of this study was to define the WIM 3-D crustal structure by modelling eight lithospheric sections, using a methodology based on the integration of seismic, wells and gravity data. The continuous nature of gravity data allowed us to propose an improved mapping of tectonic domains within the WIM showing the limits between proximal, necking, hyperthinned, exhumed mantle and oceanic areas.

The methodology used to analyze the 3D structure of the WIM and the mapping of its tectonic domains has involved the following stages:

1. The performance of gravity forward-modeling on existing seismic sections and well data.
2. The construction of longitudinal and/or transverse gravity models calibrated in the previous models, forming a mesh as regular as possible.
3. The definition of the tectonic domains and their limits in all gravity models.
4. The calculation of the BA THD and dZ gradients along the entire margin, identifying its characteristics in each tectonic domain, and the gravity features of the limits.
5. The mapping of the limits between the tectonic domains following the gravity gradients.

The main observations of this work can be summarized as follow:

1. We have mapped the crustal domains along all the WIM using calibrated gravity models and also gravity gradients (THD and dZ). This methodology is likely to be applicable in other magma poor margin; for example the Angola-Gabon rifted system, based on the results of previous published work (e.g. Péron-Pinvidic et al. 2015; Fernandez et al. 2020). Detailed interpretation of passive margin structure integrating all available data and including continuous potential data results in more sturdy interpretations than relying on a single source (e.g. seismic). This makes it also possible to contemplate correlations with domains over which scarce seismic data is available.
2. The WIM has a complex extensional structure, developed as a linear margin in SW Iberia, but branched into two main rift arms in NW Iberian margin. This pattern is locally offset by Mesozoic transfer structures and by Cenozoic compressional structures that modifies previous extensional domains.
3. The limit between the northern and southern sectors follows a NW–SE orientation, clearly observed on the BA gradient maps. This limit has the same trend that the main Variscan fabric presents in the onshore continental crust.
4. Two possible transfer zones can be highlight on this work with NW–SE orientation that separate the three classical segments of the WIM.

Beyond the particular interpretation of each margin, this methodology can also help us better understand the 3D kinematics of conjugate margins and have a critical impact on plate restoration in the early stages of their formation.

Acknowledgments First author was supported by a Ph. D grant from Repsol Exploración (Madrid) and partially financially funded by the I+D CARESOIL-CM (S2018/EMT-4317) and MARIBNO projects (PGC2018-095999-B-I00). The authors wish to thank anonymous reviewers for their thoughtful reviews that have greatly helped us to improve the quality of the paper. Geosoft Oasis Montaj and GM-SYS has been used for potential field interpretation and gravity 2-D modelling respectively. Maps and figures have been performed using GMT software (Wessel and Luis, 2017).

Author contributions CG: Conceptualization, Writing—Original Draft, Writing—Review & Editing, Methodology, Formal analysis, Investigation, Visualization. AM-M: Conceptualization, Writing—Original Draft, Writing—Review & Editing, Methodology, Formal analysis, Investigation, Visualization, Supervision. AJO: Conceptualization, Writing—Review & Editing, Formal analysis, Supervision. OF: Conceptualization, Writing—Review & Editing, Formal analysis, Supervision. MD: Formal analysis, Visualization, Review.

Funding First author was supported by a Ph. D grant from Repsol Exploración (Madrid) and partially financially funded by the I+D CARESOIL-CM (S2018/EMT-4317) and MARIBNO projects (PGC2018-095999-B-I00).

Declarations

Conflict of interest The authors declare that they have no known competing financial interests or personal relationships that could have appeared to influence the work reported in this paper.

References

- Afilhado A, Matias L, Shiobara H, Hirn A, Mendes-Victor L, Shimamura H (2008) From unthinned continent to ocean: the deep structure of the West Iberia passive continental margin at 38°N. *Tectonophysics* 458(1–4):9–50. <https://doi.org/10.1016/j.tecto.2008.03.002>
- Alves TM, Moita C, Sandnes F, Cunha T, Monteiro JH, Pinheiro LM (2006) Mesozoic-Cenozoic evolution of North Atlantic continental-slope basins: the Peniche basin, western Iberian margin. *AAPG Bull* 90:31–60
- Alves TM, Moita C, Cunha T, Ullnaess M, Myklebust R, Monteiro JH, Manupella G (2009) Diachronous evolution of Late Jurassic-Cretaceous continental rifting in the northeast Atlantic (West Iberian Margin). *Tectonics*. <https://doi.org/10.1029/2008TC002337>
- Amigo-Marx B, Fernández O, Zamora G, Poblet J, Oláiz A (2019) From large to small scale for reducing uncertainty in the structure and evolution of the Western Iberia margin. *Geophys Res Abstr* 21:1
- Ayala C (2013) A new compilation of gravity data over the Iberian Peninsula and surrounding areas. Internal Report TopoIberia project (Consolider-Ingenio). IGME, New York
- Baldy P (1977) Géologie du plateau continentale portugais (au Sud du cap de Sines). PhD, Université Pierre et Marie Curie, Paris
- Banda E, Torné M, The Iberian Atlantic Margins Group (1995) Iberian Atlantic margins group investigates deep structure of ocean margins. *Eos Trans AGU* 76:25–29. <https://doi.org/10.1029/EO076i003p00025>
- Barton PJ (1986) The relationship between seismic velocity and density in the continental crust—a useful constraint? *Geophys J Roy Astron Soc* 87(1):195–208. <https://doi.org/10.1111/j.1365-246X.1986.tb04553.x>
- Beslier MO, Cornen G, Girardeau J (1996) Tectono-metamorphic evolution of peridotites from the ocean/continent of the Iberia Abyssal Plain margin. *Proc ODP Sci Results* 149:397–412
- Blakely RJ (1996) Potential theory in gravity and magnetic applications. Cambridge University Press, Cambridge
- Boillot G (1990) LUSIGAL cruise, RV Le Suroît. <https://doi.org/10.17600/90003211>
- Boillot G, Malod J (1988) The north and north-west Spanish continental margin: a review. *Revista de la Sociedad Geológica de España* 1:295–316
- Boillot G, Recq M, Winterer EL, Applegate J, Baltuck M, Bergen JA et al (1987) Tectonic denudation of the upper mantle along passive margin: A model based on drilling results (Ocean Drilling Program leg 103, western Galicia margin, (Spain). *Tectonophysics* 132(4):335–342. [https://doi.org/10.1016/0040-1951\(87\)90352-0](https://doi.org/10.1016/0040-1951(87)90352-0)
- Boillot G, Beslier MO, Krawczyk CM, Rappin D, Reston TJ (1995) The formation of passive margins: constraints from the crustal structure and segmentation of the deep Galicia margin, Spain. In: Scrutton RA et al (eds) *The tectonics, sedimentation and paleoceanography of the North Atlantic Region*. Geological Society, Special Publications, London, pp 71–91
- Brocher TM (2005) Empirical relations between elastic wave speeds and density in the Earth's crust. *Bull Seismol Soc Am* 95(6):2081–2092
- Bronner A, Sauter D, Manatschal G, Péron-Pinvidic G, Munsch M (2011) Magmatic breakup as an explanation for magnetic anomalies at magma-poor rifted margins. *Nat Geosci* 4:549–553. <https://doi.org/10.1038/NGEO1201>
- Cadenas P, Fernández-Viejo G, Pulgar JA, Tugend J, Manatschal G, Minshull TA (2018) Constraints imposed by rift inheritance on the compressional reactivation of a hyperextended margin: mapping rift domains in the North Iberian margin and in the Cantabrian Mountains. *Tectonics* 37:758–785. <https://doi.org/10.1002/2016TC004454>
- Carbó A, Muñoz A, Llanes P, Álvarez J, ZEE Working Group (2003) Gravity analysis offshore the Canary Islands from a systematic survey. *Mar Geophys Res* 24:113–127
- Catalán M, Galindo-Zaldívar J, Davila JM, Martos YM, Maldonado A, Gambôa L, Schreider AA (2013) Initial stages of oceanic spreading in the Bransfield Rift from magnetic and gravity data analysis. *Tectonophysics* 585:102–112
- Christensen NI, Mooney WD (1995) Seismic velocity structure and composition of the continental crust: a global view. *J Geophys Res* 100:9761–9788. <https://doi.org/10.1029/95JB00259>
- Clark SA, Sawyer DS, Austin JA Jr., Christeson GL, Nakamura Y (2007) Characterizing the Galicia Bank-Southern Iberia Abyssal Plain rifted margin segment boundary using multichannel seismic and ocean bottom seismometer data. *J Geophys Res* 112:B03408. <https://doi.org/10.1029/2006JB004581>
- Córdoba D, Banda E, Ansoorge J (1987) The Hercynian crust in north-western Spain: a seismic survey. *Tectonophysics* 132(4):321–333. [https://doi.org/10.1016/0040-1951\(87\)90351-9](https://doi.org/10.1016/0040-1951(87)90351-9)
- Cowie L, Kusznir N, Manatschal G (2015) Determining the COB location along the Iberian margin and Galicia Bank from gravity anomaly inversion, residual depth anomaly and subsidence analysis. *Geophys J Int* 203(2):1355–1372. <https://doi.org/10.1093/gji/ggv367>
- Cunha PP (1992) Estratigrafia e sedimentologia dos depósitos do Cretácico Superior e Terciário de Portugal Central, al este de Coimbra. Ph.D. Thesis, Univ. Coimbra, 262 pp
- Cunha PP, Pimentel NL, Pereira DI (2000) Assinatura tectono-sedimentar do auge da compressão bética em Portugal, A descontinuidade Valesiano terminal-Turoliano. *Ciências da Terra* 14:61–72
- Curtis ML (1999) Structural and kinematic evolution of a Miocene to Recent sinistral restraining bend: the Montejunto massif, Portugal. *J Struct Geol* 21:39–54. [https://doi.org/10.1016/S0191-8141\(98\)00095-9](https://doi.org/10.1016/S0191-8141(98)00095-9)
- Davis M, Kusznir N (2004) Depth-dependent lithospheric stretching at rifted continental margins. *Proc NSF Rifted Margins Theor Inst* 1:92–136
- De Bruijne CH, Andriessen PAM (2002) Far field effects of Alpine plate tectonism in the Iberian microplate recorded by fault-related denudation in the Spanish Central System. *Tectonophysics* 349:161–184. [https://doi.org/10.1016/S0040-1951\(02\)00095-9](https://doi.org/10.1016/S0040-1951(02)00095-9)
- De Vicente G, Cunha PP, Muñoz-Martín A, Cloetingh SAPL, Olaiz A, Vegas R (2018) The Spanish-Portuguese Central System: an example of intense intraplate deformation and strain partitioning. *Tectonics*. <https://doi.org/10.1029/2018TC005204>
- De la Muela AS, Cascone L, Muñoz A, Mantilla A, Arnáiz A (2015) New insights on Peniche Basin (West Iberian Margin): crustal structure based on gravity data interpretation. Conference paper. 77th EAGE Conference & exhibition 2015 IFEMA Madrid, Spain, 1–4 June 2015. <https://doi.org/10.3997/2214-4609.201412975>
- Dean SM, Minshull TA, Whitmarsh RB, Loudon KE (2000) Deep structure of the ocean-continent transition in the southern Iberia Abyssal Plain from seismic refraction profiles: the IAM-9 transect at 40° 20' N. *J Geophys Res* 105:5859–5885

- Dentith M, Mudge ST (2014) Geophysics for the mineral exploration geoscientist. Cambridge University Press, Cambridge
- Dewey JF, Helman ML, Turco E, Hutton DHW, Knott SD (1989) Kinematics of the western Mediterranean. In: Coward MP, Dietrich D, Park RG (eds) Alpine tectonics, special publication, vol 45. Geological Society of London, London, pp 265–283
- Diaz J, Gallart J, Carbonell R (2016) Moho topography beneath the Iberian-western Mediterranean region mapped from controlled-source and natural seismicity surveys. *Tectonophysics* 692A:74–85. <https://doi.org/10.1016/j.tecto.2016.08.023>
- Doré T, Lundin E (2015) Research focus: hyperextended continental margins—knowns and unknowns. *Geology* 43(1):95–96. <https://doi.org/10.1130/focus012015.1>
- Dragoi-Stavar D, Hall D (2009) Gravity modelling of the ocean-continent transition along the South Atlantic margins. *J Geophys Res* 114:B09401. <https://doi.org/10.1029/2008JB006014>
- Druet M, Muñoz-Martín A, Granja-Bruña JL, Carbó-Gorosabel A, Acosta J, Llanes P, Ercilla G (2018) Crustal structure and continent-ocean boundary along the Galicia continental margin (NW Iberia): insights from combined gravity and seismic interpretation. *Tectonics* 37(5):1576–1604
- Druet M, Muñoz-Martín A, Granja-Bruña JL, Carbó-Gorosabel A, Acosta J, Llanes P, Catalán M, Maestro A, Bohoyo F, Matín-Dávila J (2019) Bouguer anomalies of the NW Iberian continental margin and the adjacent abyssal plains. *J Maps* 15(2):635–641. <https://doi.org/10.1080/17445647.2019.1644214>
- Eagles G, Pérez-Díaz L, Scarselli N (2015) Getting over continent ocean boundaries. *Earth Sci Rev*. <https://doi.org/10.1016/j.earscirev.2015.10.009>
- Fernandez O, Olaiz A, Cascone L, Hernandez P, de Pereira AF, Tritilla J, Ingles M, Aida B, Pinto I, Rocca R, Sanders C, Herrá A, Tur N (2020) Geophysical evidence for breakup volcanism in the Angola and Gabon passive margins. *Mar Pet Geol*. <https://doi.org/10.1016/j.marpetgeo.2020.104330>
- González A, Córdoba D, Vales D (1999) Seismic crustal structure of Galicia continental margin, NW Iberian Peninsula. *Geophys Res Lett* 26:1061–1064. <https://doi.org/10.1029/1999GL900193>
- Haase C, Ebbing J, Funck T (2016) A 3D regional crustal model of the NE Atlantic based on seismic and gravity data. In: Péron-Pinvidic G, Hopper JR, Stoker T, Gaina C, Doornebal H, Funck T, Ártung U (eds) The NE Atlantic region: a reappraisal of crustal structure, tectonostratigraphy and magmatic evolution. Geological Society, Special Publications, London
- Hafid M, Ait SA, Bally AW (2000) The western termination of the Jbileh—high Atlas system (Offshore Essaouira Basin, Morocco). *Mar Pet Geol* 17:431–443. [https://doi.org/10.1016/S0264-8172\(98\)00082-8](https://doi.org/10.1016/S0264-8172(98)00082-8)
- Hellinger SJ, Sclater JG (1983) Some comments on two-layer extensional models for the evolution of sedimentary basins. *J Geophys Res* 88:8251–8269. <https://doi.org/10.1029/JB088iB10p08251>
- Henning AT, Sawyer DS, Templeton DC (2004) Exhumed upper mantle within the ocean-continent transition on the northern West Iberia margin: evidence from pre-stack depth migration and total tectonic subsidence analyses. *J Geophys Res*. <https://doi.org/10.1029/2003JB002526>
- Hinze WJ, Frese RRBV, Saad AH (2013) Gravity and magnetic exploration: principles, practices, and applications. Cambridge University Press. <https://doi.org/10.1017/CBO9780511843129>
- Hubbard R, Pape J, Roberts DE (1985) Depositional sequence mapping as a technique to establish tectonic and stratigraphic framework and evaluate hydrocarbon potential on a passive continental margin. In: Berg OR, Woolverton DG (eds) Seismic stratigraphy II: an integrated approach, vol 39. AAPG Memoirs, Tulsa, pp 79–91
- Jiménez-Munt I, Fernández M, Vergés J, Afonso JC, García-Castellanos D, Fullea J (2010) Lithospheric structure of the Gorringe Bank: insights into its origin and tectonic evolution. *Tectonics*. <https://doi.org/10.1029/2009TC002458>
- Kane MF (1962) A comprehensive system of terrain corrections using a digital computer. *Geophysics* 27(4):455–462. <https://doi.org/10.1190/1.1439044>
- Kornprobst J, Chazot G (2016) Peridotites and mafic igneous rocks at the foot of the Galicia margin: an oceanic or continental lithosphere? A discussion. *Boletín Geológico y Minero* 127(2/3):317–332
- Krawczyk CM, Reston TJ, Beslier MO, Boillot G (1996) Evidence for detachment tectonics on the Iberia abyssal plain rifted margin. In: Whitmarsh RB et al (eds) Proceedings of the Ocean Drilling Program, scientific results, vol 149. Ocean Drilling Program, College Station, pp 603–615. <https://doi.org/10.2973/odp.proc.sr.149.244.1996>
- Lavier L, Ball PJ, Manatschal G, Heumann MJ, McDonald J, Matts V, Schneider C (2019) Heatflow, magmatism, hydrothermal circulation, and rift domain mapping: a new understanding of crustal-scale rift-related processes within the Kwanza Basin, Angola. *Geochem Geophys Geosyst*. <https://doi.org/10.1029/2019GC008580>
- Lesur V, Hamoudi M, Choi Y, Dymant J, Thébaud E (2016) Building the second version of the world digital magnetic anomaly map (WDMAM). *Earth Planets Space* 68:1–13
- Ludwig WJ, Nafe JE, Drake CL (1970) Seismic refraction. In: Maxwell AE (ed) The sea, vol 4. Wiley-Interscience, New York, pp 53–84
- Lymer G, Cresswell DJF, Reston TJ, Bull JM, Sawyer DS, Morgan JK, Stevenson C, Causer A, Minshull TA, Shillington DJ (2019) 3D development of detachment faulting during continental breakup. *Earth Planet Sci Lett* 515:90–99. <https://doi.org/10.1016/j.epsl.2019.03.018>
- Manatschal G, Bernoulli D (1999) Architecture and tectonic evolution of non-volcanic margins: present day Galicia and ancient Adria. *Tectonics* 18:1099–1119. <https://doi.org/10.1029/1999TC900041>
- Manatschal G, Froitzheim N, Rubenach MJ, Turrin B (2001) The role of detachment faulting in the formation of an ocean-continent transition: insights from the Iberia Abyssal Plain. In: Wilson RCL, Whitmarsh RB, Taylor B, Froitzheim N (eds) Non-Volcanic Rifting of continental margins: evidence from land and sea, vol 187. Geol Soc (London) Spec Publ, London, pp 405–428. <https://doi.org/10.1144/GSL.SP.2001.187.01.20>
- Manatschal G, Lavier L, Chenin P (2015) The role of inheritance in structuring hyperextended rift systems: some considerations based on observations and numerical modelling. *Gondwana Res* 27:140–164
- Matos JED (1979) Estudo de microfácies de rochas da vertente continental portuguesa. Serviços Geológicos de Portugal, Lisbon
- Mauffret A, Mougnot D, Miles PR, Malod JA (1989) Results from multichannel reflection profiling of the Tagus Abyssal Plain (Portugal)—Comparison with the Canadian Margin. In: Tankard AJ, Balkwill HR (eds) Extension tectonics and stratigraphy of the North Atlantic margins, vol 46. AAPG Memoirs, Tulsa, pp 379–393
- McKenzie D (1978) Some remarks on the development of sedimentary basins. *Earth Planet Sci Lett* 40:25–32
- Miles PR, Verhoeve J, Macnab R (1996) Compilation of magnetic anomaly chart West of Iberia. In: Whitmarsh RB, Sawyer D, Klaus A, Masson DG (eds) Proceedings of the ocean drilling program scientific results, vol 149. Ocean Drilling Program, College Station, pp 659–663. <https://doi.org/10.2973/odp.proc.sr.149.242.1996>
- Miranda R (2010) Petrogenesis and geochronology of the Late Cretaceous alkaline magmatism in the west Iberian Margin. PhD thesis, University of Lisbon, Lisbon
- Mohn G, Manatschal G, Beltrando M, Masini E, Kuszniir N (2012) Necking of continental crust in magma-poor rifted margins:

- evidence from the fossil Alpine Tethys margins. *Tectonics* 31:TC1012. <https://doi.org/10.1029/2011TC002961>
- Mohn G, Karner GD, Manatschal G, Johnson CA (2015) Structural and stratigraphic evolution of the Iberia-Newfoundland hyperextended rifted margin: a quantitative modelling approach. In: Gibson GM, Froure, Manatschal G (eds) *Sedimentary basins and crustal processes at continental margins: from modern hyperextended margins to deformed ancient analogues*. Geological Society of London, Special Publications, London. <https://doi.org/10.1144/SP413.9>
- Mougenot D, Monteiro JH, Dupeuble PA, Malod JA (1979) La marge continentale sud-portugaise: évolution nstructurale et sédimentaire. *Ciências da Terra* 5:223–246
- Murillas J, Mougenot DG, Boillot G, Comas MC, Banda E, Mauffret A (1990) Structure and evolution of the Galicia interior basin (Atlantic western Iberian continental margin). *Tectonophysics* 184:297–319
- Nagy D (1966) The gravitational attraction of a right rectangular prism. *Geophysics* 31(2):362–371
- Nirrengarten M, Manatschal G, Tugend J, Kuszniir NJ, Sauter D (2017) Nature and origin of the J-magnetic anomaly offshore Iberia–Newfoundland: implications for plate reconstructions. *Terra Nova* 29:20–28. <https://doi.org/10.1111/ter.12240>
- Nirrengarten M, Manatschal G, Tugend J, Kuszniir N, Sauter D (2018) Kinematic evolution of the southern North Atlantic: implications for the formation of hyperextended rift systems. *Tectonics*. <https://doi.org/10.1002/2017TC004495>
- ODP Leg 173 Shipboard Scientific Party (1998) Drilling reveals transition from continental breakup to early magmatic crust, EOS, Transactions, AGU, 79, pp 180–181
- Osmundsen PT, Redfield T (2011) Crustal taper and topography at passive continental margins. *Terra Nova* 23:349–361. <https://doi.org/10.1111/j.1365-3121.2011.01014.x>
- Peace AL, Welford JK, Ball PJ, Nirrengarten M (2019) Deformable plate tectonic models of the southern North Atlantic: insights into rift-related deformation and magmatism. *Geodynamics*. <https://doi.org/10.1016/j.jog.2019.05.005>
- Pereira R, Alves TM (2011) Margin segmentation prior to continental breakup: a seismic–stratigraphic record of multiphased rifting in the North Atlantic. *Tectonophysics* 505:17–34. <https://doi.org/10.1016/j.tecto.2011.03.011>
- Pereira R, Alves TM (2012) Tectono-stratigraphic signature of multiphase drifting on divergent margins (deep-offshore Southwest Iberia, North Atlantic). *Tectonics* 31:TC4001. <https://doi.org/10.1029/2011TC003001>
- Pereira R, Alves TM, Mata J (2017) Alternating crustal architecture in West Iberia: a review of its significance in the context of NE Atlantic rifting. *J Geol Soc Lond Spec Publ* 174(3):522–540
- Pérez-Gussinyé M, Reston TJ (2001) Rheological evolution during extension at nonvolcanic rifted margins: onset of serpentinization and development of detachments leading to continental breakup. *J Geophys Res* 106:3961–3975
- Pérez-Gussinyé M, Ranero CR, Reston TJ (2003) Mechanisms of extension at non-volcanic margins: evidence from the Galicia interior basin, west of Iberia. *J Geophys Res* 108(B5):2245. <https://doi.org/10.1029/2001JB000901>
- Péron-Pinvidic G, Manatschal G (2009) The final rifting evolution at deep magma-poor passive margins from Iberia-Newfoundland: a new point of view. *Int J Earth Sci* 98:1581–1597. <https://doi.org/10.1007/s00531-008-0337-9>
- Péron-Pinvidic G, Manatschal G, Osmundsen PT (2013) Structural comparison of archetypal Atlantic rifted margins: a review of observations and concepts. *Mar Pet Geol* 43:21–47. <https://doi.org/10.1016/j.marpetgeo.2013.02.002>
- Péron-Pinvidic G, Manatschal G, Masini E, Sutra E, Flament JM, Haupeit I, Unternehr P (2015) Unravelling the along-strike variability of the Angola-Gabon rifted margin: a mapping approach. In: Sabato Ceraldi T, Hodkinson RA, Backe G (eds) *Petroleum geoscience of the West Africa Margin*, vol 438. Geological Society of London, Special Publication, London, pp 49–76
- Pickup SLB, Whitmarsh RB, Fowler CMR, Reston TJ (1996) Insight into the nature of the ocean-continent transition west of Iberia from a deep multichannel seismic reflection profile. *Geology* 24(12):1079–1082
- Pinheiro LM, Whitmarsh RB, Miles PR (1992) The ocean continent boundary off the western continental-margin of Iberia 2. Crustal structure in the Tagus Abyssal- Plain. *Geophys J Int* 109(1):106–124
- Pinheiro LM, Wilson RCL, Pena dos Reis R, Whitmarsh RB, Ribeiro A (1996) The Western Iberia Margin: a geophysical and geological overview. In: Whitmarsh RB, Sawyer DS, Klaus A, Masson DG (eds) *Proceedings of the Ocean Drilling Program, scientific results*, vol 149. Ocean Drilling Program, College Station
- Pinto VH, Manatschal G, Karpoff AM, Ulrich M, Viana AR (2016) Seawater storage and element transfer associated with mantle serpentinization in magma-poor rifted margins: a quantitative approach. *Earth Planet Sci Lett* 459:227–237. <https://doi.org/10.1016/j.epsl.2016.11.023>
- Ramos A, Fernandez O, Muñoz JA, Terrinha O (2017) Impact of basin structure and evaporite distribution on salt tectonics in the Algarve Basin, Southwest Iberian margin. *Mar Pet Geol* 43:21–47
- Rasmussen ES, Lomholt S, Andersen C, Vejbaek O (1998) Aspects of the structural evolution of the Lusitanian basin in Portugal and the shelf slope area offshore Portugal. *Tectonophysics* 300:199–225
- Reguzzoni M, Sampietro D (2015) GEMMA: an Earth crustal model based on GOCE satellite data. *Int J Appl Earth Obs Geoinf* 35:31–43. <https://doi.org/10.1016/j.jag.2014.04.002>
- Reston TJ (2009) The structure, evolution and symmetry of the magma-poor rifted margins of the North and Central Atlantic: a synthesis. *Tectonophysics* 468:6–27. <https://doi.org/10.1016/j.tecto.2008.09.002>
- Reston T, McDermott K (2014) An assessment of the cause of the ‘extension discrepancy’ with reference to the west Galicia margin. *Basin Res* 26(1):135–153. <https://doi.org/10.1111/bre.12042>
- Reston TJ, Leythaeuser T, Booth-Rea G, Sawyer D, Klaeschen D, Long C (2007) Movement along a low-angle normal fault: the S reflector west of Spain. *Geochem Geophys Geosyst* 8:Q06002. <https://doi.org/10.1029/2006GC001437>
- Ribeiro A, Kullberg MC, Kullberg JC, Manuppella G, Phipps S (1990) A review of Alpine tectonics in Portugal: Foreland detachment in basement and cover rocks. *Tectonophysics* 184(3–4):357–366. [https://doi.org/10.1016/0040-1951\(90\)90448-H](https://doi.org/10.1016/0040-1951(90)90448-H)
- Russell SM, Whitmarsh RB (2003) Magmatism at the west Iberia non-volcanic rifted continental margin: evidence from analyses of magnetic anomalies. *Geophys J Int* 154:706–730. <https://doi.org/10.1046/j.1365-246X.2003.01999.x>
- Sallares V, Martínez-Loriente S, Prada M, Gracia E, Ranero CR, Gutscher MA, Bartolome R, Gailler A, Dañoibeitia JJ, Zitellini N (2013) Seismic evidence of exhumed mantle rock basement at the Gorringer Bank and the adjacent Horseshoe and Tagus abyssal plains (SW Iberia). *Earth Planet Sci Lett* 365:120–131. <https://doi.org/10.1016/j.epsl.2013.01.021>
- Sampietro D, Reguzzoni M, Negretti N (2013) The GEMMA crustal model: first validation and data distribution. *ESA SP-722*
- Sanchez G, Merle R, Hirschberger F, Thinond I, Girardeau J (2019) Post-spreading deformation and associated magmatism along the Iberia-Morocco Atlantic margins: insight from submarine volcanoes of the Tore-Madeira Rise. *Mar Geol* 407:76–93. <https://doi.org/10.1016/j.margeo.2018.10.011>

- Sawyer DS, Whitmarsh RB, Klaus A et al (1994) Proc. ODP, initial reports, vol 149. Ocean Drilling Program, College Station
- Schermerhorn LJJ, Priem HNA, Boelrijk NAIM, Hebeda EH, Verdurmen EAT, Verschure RH (1978) Age and origin of the Messejana dolerite fault–dike system (Portugal and Spain) in the light of the opening of the North Atlantic Ocean. *J Geol* 86:299–309
- Sibuet JC, Louvel V, Whitmarsh RB, White RS, Horsefield SJ, Sichler B, León P, Recq M (1995) Constraints on rifting processes from refraction and deep-tow magnetic data: the example of the Galicia continental margin (West Iberia). In: Banda E et al (eds) *Rifted ocean-continent boundaries*. Kluwer Academic Publishers, Dordrecht, pp 197–217. https://doi.org/10.1007/978-94-011-0043-4_11
- Sibuet JC, Srivastava SP, Spakman W (2004) Pyrenean orogeny and plate kinematics. *J Geophys Res Solid Earth*. <https://doi.org/10.1029/2003JB002514>
- Sibuet JC, Srivastava SP, Manatschal G (2007) Exhumed mantle-forming transitional crust in the Newfoundland-Iberia rift and associates magnetic anomalies. *J Geophys Res* 112:B06105. <https://doi.org/10.1029/2005JB003856>
- Smith WHF, Wessel P (1990) Gridding with continuous curvature in tension. *Geophysics* 55:293–305
- Srivastava SP, Schouten H, Roest WR, Kiltgord KD, Kovacs LC, Verhoef J, Macnab R (1990) Iberian plate kinematics: a jumping plate boundary between Eurasia and Africa. *Nature* 344:756–759
- Stanton N, Manatschal G, Autin J, Sauter D, Maia M, Viana A (2016) Geophysica Ifingerprints of hyper-extended, exhumed and embryonic oceanic domains: the example for the Iberia-Newfoundland rifted margins. *Mar Geophys Res*. <https://doi.org/10.1007/s11001-016-9277-0>
- Steckler MS, Watts AB (1978) Subsidence of the Atlantic-type continental margin off New York. *Earth Planet Sci Lett* 41:1–13. [https://doi.org/10.1016/0012-821X\(78\)90036-5](https://doi.org/10.1016/0012-821X(78)90036-5)
- Sutra E, Manatschal G (2012) How does the continental crust thin in a hyperextended rifted margin? Insights from the Iberia margin. *Geology* 40(2):139–142. <https://doi.org/10.1130/G32786.1>
- Sutra E, Manatschal G, Mohn G, Unternehr P (2013) Quantification and restoration of extensional deformation along the Western Iberia and Newfoundland rifted margins. *Geochem Geophys Geosyst*. <https://doi.org/10.1002/ggge.20135>
- Talwani M, Heirtzler JR (1964) Computation of magnetic anomalies caused by two dimensional bodies of arbitrary shape. In: Parks GA (ed) *Computers in the mineral industries, part 1, vol 9*. Stanford University publications, Geological Sciences, Palo Alto, pp 464–480
- Talwani M, Worzel JL, Landisman M (1959) Rapid gravity computations for two dimensional bodies with application to the Mendocino submarine fracture zone. *J Geophys Res* 64:49–59. <https://doi.org/10.1029/JZ064i001p00049>
- Tucholke BE, Ludwig WJ (1982) Structure and origin of the J anomaly Ridge, western North Atlantic Ocean. *J Geophys Res* 87(B11):9389–9407
- Tucholke BE, Sibuet JC (2012) Problematic plate reconstruction. *Nat Geosci* 5(10):676–677. <https://doi.org/10.1038/ngeo1596>
- Tucholke BE, Sawyer DS, Sibuet JC (2007) Breakup of the Newfoundland-Iberia rift. In: Karner GD, Manatschal G, Pinheiro LM (eds) *Imaging, mapping and modelling continental lithosphere extension and breakup, vol 282*. Geological Society of London, Special Publications, London, pp 9–49
- Tugend J, Manatschal G, Kuszniir NJ, Masini E, Mohn G, Thion J (2014) Formation and deformation of hyperextended rift systems: insights from rift domain mapping in the Bay of Biscay-Pyrenees. *Tectonics*. <https://doi.org/10.1002/2014TC003529>
- Tugend J, Manatschal G, Kuszniir NJ, Masini E (2015) Characterizing and identifying structural domains at rifted continental margins: application to the Bay of Biscay margins and its Western Pyrenean fossil remnants. *Geol Soc Lond Spec Publ* 413(1):171. <https://doi.org/10.1144/SP413.3>
- Vázquez JT, Medialdea T, Ercilla G, Somoza L, Estrada F, Fernández Puga MC et al (2008) Cenozoic deformational structures on the Galicia Bank Region (NW Iberian continental margin). *Mar Geol* 249(1–2):128–149. <https://doi.org/10.1016/j.margeo.2007.09.014>
- Vergés J (1999) Estudi geològic del vessant sud del Pirineu oriental i central. *Evolució cinemàtica en 3D*. Servei Geològic Monografia Tècnica 7:192
- Welford JK, Smith JA, Hall J, Deemer S, Srivastava SP, Sibuet JC (2010) Structure and rifting evolution of the northern Newfoundland Basin from Erable multichannel seismic reflection profiles across the southeastern margin of Flemish Cap. *Geophys J Int* 180(3):976–998
- Wessel P, Luis JF (2017) The GMT/MATLAB toolbox. *Geochem Geophys Geosyst* 18(2):811–823
- Whitmarsh RB, Miles PR (1995) Models of the development of the West Iberia rifted continental margin at 40°30'N deduced from surface and deep-tow magnetic anomalies. *J Geophys Res* 100:3789–3806. <https://doi.org/10.1029/94JB02877>
- Whitmarsh RB, Sawyer DS (1996) The ocean/continent transition beneath the Iberia Abyssal Plain and continental rifting to sea-floor-spreading processes. In: Whitmarsh RB, Sawyer DS, Klaus A (eds) *Proceedings of the Ocean Drilling Program, scientific results, vol 149*. Ocean Drilling Program, College Station, pp 713–733
- Whitmarsh RB, Wallace PJ (2001) The rift-to-drift development of the West Iberia nonvolcanic continental margin: A summary and review of the contribution of ocean drilling program leg 173. In: Beslier MO, Whitmarsh RB, Wallace PJ, Girardeau J (eds) *Proceedings of the Ocean Drilling Program, scientific results, vol 173*. Ocean Drilling Program, College Station, pp 1–36
- Whitmarsh RB, Miles PR, Pinheiro M (1990) The seismic velocity structure of some NE Atlantic continental rise sediments; a lithification index? *Geophys J Int* 101:367–378
- Whitmarsh RB, Pinheiro LM, Miles PR, Recq M, Sibuet JC (1993) Thin crust at the western Iberia ocean-continent transition and ophiolites. *Tectonics* 12–5:1230–1239. <https://doi.org/10.1029/93TC00059>
- Whitmarsh RB, White RS, Horsefield SJ, Sibuet JC, Recq M, Louvel V (1996) The ocean-continent boundary off the western continental margin of Iberia: crustal structure west of Galicia Bank. *J Geophys Res* 101:28291–28314. <https://doi.org/10.1029/96JB02579>
- Whitmarsh RB, Beslier MO, Wallace JP (1998) *Proceedings of the Ocean Drilling Program, initial reports, vol 173*. Ocean Drilling Program, College Station
- Whittaker J, Goncharov A, Williams S, Müller RD, Leitchenkov G (2013) Global sediment thickness dataset updated for the Australian-Antarctic Southern Ocean. *Geochem Geophys Geosyst* 14(8):3297–3305. <https://doi.org/10.1002/ggge.20181>
- Wilson RCL, Hiscott RN, Willis MG, Gradstein PM (1989) The Lusitanian Basin of west-central Portugal: Mesozoic and Tertiary tectonic stratigraphic and subsidence history. In: Tankard AJ, Balkwill HR (eds) *Extensional tectonics and stratigraphy of the North Atlantic Margins, vol 46*. AAPG Memoirs, Tulsa, pp 341–361
- Won IJ, Bevis M (1987) Computing the gravitational and magnetic anomalies due to a polygon: algorithms and Fortran subroutines. *Geophysics* 52:232–238
- Zelt CA, Sain K, Naumenko JV, Sawyer DS (2003) Assessment of crustal velocity models using seismic refraction and reflection tomography. *Geophys J Int* 153(3):609–626
- Zitellini N, Gràcia E, Matias L, Terrinha P, Abreu MA, De Alteriis G, Henriot JP, Dañoibeitia JJ, Masson DG, Mulder T (2009) The

quest for the Africa-Eurasia plate boundary west of the Strait of Gibraltar. *Earth Planet Sci Lett* 280(1–4):13–50. <https://doi.org/10.1016/j.epsl.2008.12.005>

Publisher's Note Springer Nature remains neutral with regard to jurisdictional claims in published maps and institutional affiliations.